



W 4 D888c 2007  
Dumka, Disha  
Cross-bridge kinetics of  
cardiac myofibrils carrying

UNTHSC - FW



M03JWG



LEWIS LIBRARY  
UNT Health Science Center  
3500 Camp Bowie Blvd.  
Ft. Worth, Texas 76107-2699







Dumka, Disha., Cross-bridge kinetics of cardiac myofibrils carrying myopathy-causing mutation. Doctor of Philosophy (Biochemistry and Molecular Biology), May 2007, 98 pp., 8 tables, 23 illustrations, and bibliography: 102 titles.

Familial hypertrophic cardiomyopathy is a disease characterized by left ventricular hypertrophy and myofibrillar disarray. It is caused by mutations in sarcomeric proteins, including the ventricular isoform of myosin regulatory light chain (RLC). We have focused on one particular mutation of RLC- substitution of glutamic acid (E) at position 22 for lysine (K). The E22K mutation is located in the RLC  $\text{Ca}^{2+}$ -binding site. Earlier work has demonstrated that phosphorylation and  $\text{Ca}^{2+}$  binding are significantly altered by the E22K mutation. Studies with transgenic (Tg) mice have demonstrated that E22K-RLC mutation increases  $\text{Ca}^{2+}$  sensitivity of myofibrillar ATPase activity and steady-state force. However, the mechanisms for the E22K-mutated myocardium that could potentially trigger hypertrophy as seen in human patients harboring this mutation remain unclear.

In order to better understand the impact of the E22K-RLC mutation on cardiac muscle contraction, we have studied the three primary parameters which best reflect the mechanism of actomyosin cross-bridge cycling during force generation. Tau one and two ( $\tau_1$  and  $\tau_2$ ) are the mechanical parameters which measure the dissociation and rebinding time of myosin heads from actin, respectively. Tau three ( $\tau_3$ ) is an enzymatic parameter which measures the dissociation time of ADP from the active site of myosin. For this study single-turnover contraction experiments were performed on Tg (wild-type and E22K) and non-Tg mouse cardiac myofibrils.



Tau one ( $\tau_1$ ) was statistically greater in Tg-m (Tg-E22K) than in controls indicating that the E22K mutation slows down the rate of cross-bridge dissociation. However, the *in-vitro* binding experiments showed no difference in binding properties of Tg-m vs. Tg-wt myosin to fluorescently labeled actin suggesting that this was a function of genetic manipulation rather than an intrinsic change to muscle. The slight increase in  $\tau_1$  was probably caused by myofibrillar disarray. Tau two ( $\tau_2$ ) was shorter in Tg-m than in non-Tg, but the same as in Tg-wt indicating that the decrease in  $\tau_2$  of Tg hearts was probably caused by replacement of the mouse RLC for the human isoform in the transgenic mice. Tau three ( $\tau_3$ ) was the same in Tg-m and in controls indicating that the E22K mutation had no effect time of ADP dissociation from the myosin active site.

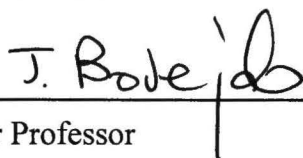
Thus the E22K mutation did not affect the three parameters that were used to study the cross-bridge kinetics of the cardiac muscle from transgenic mice carrying the E22K-RLC mutation. On extrapolating the results of this study with transgenic mice to humans, it is likely that the change in cross-bridge kinetics is not the primary trigger through which E22K-RLC mutation affects muscle contraction. However one possible limitation of this study is that the Tg-E22K mice did not completely recapitulate the human phenotype of E22K-mutation. Overall, in this study, we successfully followed the mechanical and the enzymatic events in a small population of cross-bridges (~400) in contracting Tg-m cardiac myofibrils. The characterization of motion of a small population of cross-bridges is important because the different steps of cross-bridge cycle do not become obscured and thus it becomes easy to detect any changes in the cross-bridge cycle.



CROSS-BRIDGE KINETICS OF CARDIAC MYOFIBRILS CARRYING  
MYOPATHY-CAUSING MUTATION

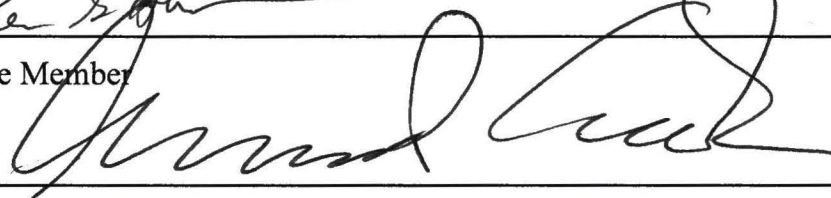
Disha Dumka, M.S.

APPROVED:

  
Major Professor

5/1/07

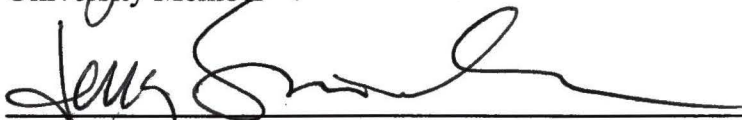
  
Committee Member

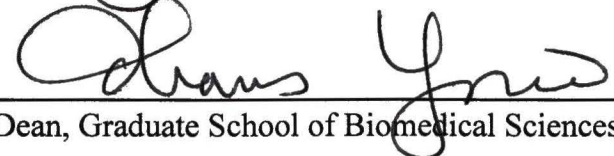
  
Committee Member

  
Committee Member

Committee Member

  
University Member

  
Chair, Department of Biochemistry and Molecular Biology

  
Dean, Graduate School of Biomedical Sciences

CROSS-BRIDGE KINETICS OF CARDIAC MYOFIBRILS CARRYING  
MYOPATHY-CAUSING MUTATION

DISSERTATION

Presented to the Graduate Council of the  
Graduate School of Biomedical Sciences

University of North Texas  
Health Science Center at Fort Worth

For the Degree of

DOCTOR OF PHILOSOPHY

By

Disha Dumka, M.S.

Fort Worth, Texas

May 2007



## TABLE OF CONTENTS

List of Abbreviations	v
List of Illustrations	vi
List of Tables	viii
<b>CHAPTER</b>	
1. INTRODUCTION	
1. Structure and Function of Skeletal Muscle	1
2. Structure and Function of Cardiac Muscle	11
3. Familial Hypertrophic Cardiomyopathy	16
4. Rationale	31
2. MATERIAL AND METHODS	
1. Methods for Studying Skeletal Muscle	43
2. Methods for Studying Cardiac Muscle	49
3. DEVELOPMENT OF EXPERIMENTAL APPROACH USING SKELETAL MUSCLE	53
4. EFFECT OF E22K-RLC MUTATION ON CARDIAC MUSCLE FUNCTION	
1. Cardiac Myofibril Measurements	62
2. Cardiac Proteins <i>In Vitro</i>	74
5. DISCUSSION	79
1. Possible Limitations of our Study	82

2. Future Directions	84
6. CONCLUSION	89

## LIST OF ABBREVIATIONS

ADP	Adenosine Diphosphate
ANOVA	Analysis of Variance
ATP	Adenosine Triphosphate
DTT	Dithiothreitol
EDTA	Ethylene-diamine-tetra-acetic acid
EGTA	Ethylene Glycol-bis( $\beta$ -aminoethyl) ether
ELC	Essential Light Chain
FHC	Familial Hypertrophic Cardiomyopathy
HCRLC	Human Cardiac RLC
I	Anisotropy
$I_{  }$	Horizontal Emission Intensity
$I_{\perp}$	Vertical Emission Intensity
5'-IAF	5'-Iodoacetoamido-fluorescein
5'-IATR	5'- Iodoacetamido-tetramethyl-rhodamine
IPTG	Isopropyl- $\beta$ -D-thiogalactoside
$K_{Ca}$	Calcium Binding Affinity
LC1	Essential Light Chain
LC2	Regulatory Light Chain
MLC	Myosin Light Chain
MLCK	Myosin Light Chain Kinase
MyHC	Myosin Heavy chain
Ni-NTA	Nickel-Nitrilotriacetic acid
PMSF	Phenylmethanesulfonyl Fluoride
RLC	Regulatory Light Chain
S1	Subfragment-1 of Myosin
SCD	Sudden Cardiac Death
SDS	Sodium Dodecyl Sulfate
SDS-PAGE	SDS Polyacrylamide Gel Electrophoresis
TFP	Tri-fluoroperazine
vRLC	Ventricular Regulatory Light Chain
$\tau_1$	Dissociation time of myosin heads from thin filaments
$\tau_2$	Re-binding time of the cross-bridges to actin
$\tau_3$	Dissociation time of ADP from the active site of myosin
$\tau$ (cardiac proteins in-vitro)	Excited State Lifetime



## LIST OF ILLUSTRATIONS

### CHAPTER I

<b>Figure 1:</b> Structure of skeletal muscle .....	3
<b>Figure 2.</b> A) Schematic representation of a myosin molecule.....	4
B) Three-dimensional structure of a chicken skeletal myosin head (S1)	
<b>Figure 3:</b> Illustration of the rotation of the lever arm during force production.....	6
<b>Figure 4:</b> Cross-Bridge cycle.....	7
<b>Figure 5:</b> Illustration of $\text{Ca}^{2+}$ -Tn-Tm regulated striated muscle contraction.....	11
and the effect of RLC phosphorylation and $\text{Ca}^{2+}$ binding	
<b>Figure 6.</b> The cardiac sarcomere comprises the contractile proteins of the.....	13
thick and thin filaments	
<b>Figure 7:</b> Cardiac sarcomere in relation to the membranous structures .....	13
responsible for intracellular $\text{Ca}^{2+}$ handling	
<b>Figure 8:</b> A, Three-dimensional representation of human cardiac RLC B, exon.....	18
organization of HCRLC and the sites of all FHC mutations identified to date	
<b>Figure 9:</b> Amino acid sequence alignment of various isoforms of .....	29
myosin regulatory light chains	
<b>Figure 10:</b> Importance of measuring single head kinetics.....	38
<b>Figure 11:</b> Schematic of the illumination volume impinging on the .....	39
muscle	

### CHAPTER III

<b>Figure 1:</b> Confocal image of fluorescently labeled skeletal fibers: Actin.....	55
labeled with FITC-phalloidin (green) (A) and myosin labeled with essential light chain coupled to IATR (red) (B) in the same muscle fiber	
<b>Figure 2:</b> Incorporation of fluorescent light chains into skeletal muscle.....	56
<b>Figure 3.</b> Time course of change of perpendicular anisotropy of muscle.....	59
labeled with Rh-Ph. Muscle is initially in rigor	
<b>Figure 4.</b> Time course of change of perpendicular anisotropy of muscle.....	61
labeled with Rh-LC1	

### CHAPTER IV

<b>Figure 1:</b> ELC purification.....	65
<b>Figure 2.</b> Confocal image of fluorescently labeled cardiac myofibrils.....	66
Myosin in myofibrils was exchanged with Rh-LC1 (A), AlexaATP (B) and Rh-phalloidin (C)	
<b>Figure 3:</b> Incorporation of Rh-LC1 into skeletal and cardiac myofibrils.....	66
<b>Figure 4.</b> Time course of change of perpendicular anisotropy of muscle.....	68
labeled with Rh-Ph	
<b>Figure 5.</b> Time course of change of perpendicular anisotropy of muscle.....	71
labeled with Rh-LC1	
<b>Figure 6.</b> Time course of change of perpendicular anisotropy of muscle.....	73
labeled with AlexaATP	
<b>Figure 7.</b> Fluorescent lifetime of fluorescein-phalloidin labeled actin.....	76
<b>Figure 8.</b> Excitation anisotropy of Rh-LC1.....	78

## LIST OF TABLES

### CHAPTER I

<b>Table 1.</b> Sarcomeric proteins and genes responsible for FHC.....	17
<b>Table 2.</b> Effect of FHC mutations and phosphorylation on the $\text{Ca}^{2+}$ binding to human cardiac RLC .....	21
<b>Table 3.</b> Effect of FHC-RLC Mutations on mechanical properties.....	24
in reconstituted muscle preparations	
<b>Table 4.</b> Comparison of mechanical and physiological properties of ..... different FHC-RLC mutations	33

### CHAPTER IV

<b>Table 1.</b> Times of dissociation ( $\tau_1$ ) of cross-bridges from actin.....	69
<b>Table 2.</b> Rates of rotation ( $1/\tau_2$ ) of the myosin lever arm.....	70
<b>Table 3.</b> Times of ADP dissociation ( $\tau_3$ ) from myosin active site.....	72
<b>Table 4.</b> Fluorescent lifetimes of binding of Tg-wt and E22K myosin to actin.....	77



## CHAPTER I

### INTRODUCTION

#### 1. Structure and Function of Skeletal Muscle

**A. Structure:** Muscles are arranged as bundles of fibers. Each skeletal muscle fiber is a single cylindrical muscle cell. Muscle can be divided into compartments called fascicles, which are separated by a connective tissue sheath called the epimysium. Within each fascicle are muscle fibers or muscle cells. Each muscle fiber contains numerous myofibrils composed of repeating sarcomere units separated by Z-discs. These sarcomere units are aligned in a sequence and are attached to each other through the Z-discs. The sarcomere is composed of both thin and thick filaments (**Figure 1**). The thin filaments are composed of actin,  $\alpha$ -tropomyosin, and troponins. The thick filaments are composed of several hundreds of myosin molecules assembled together. Myosin is the molecular motor that transduces energy from the hydrolysis of ATP (adenosine triphosphate) into directed movement to drive sarcomere shortening and muscle contraction.

Skeletal myosin is a conventional class II myosin with a molecular weight of 520 kDa. It consists of two myosin heavy chains (MyHCs) and two pairs of myosin light chains (MLCs). These chains are referred to as essential (or alkali) light chains (ELC or LC1), and regulatory (or phosphorylatable) light chains (RLC or LC-2), respectively (69, 9) (**Figure 2A**). The tail domains of myosin heavy chains associate in a rod-like,  $\alpha$ -helical coiled coil. Papain, a protease, cleaves myosin and allows the separation of a

fragment called subfragment-1 (S1), which connects only the motor/catalytic/head domain and neck/regulatory region with attached light chains (**Figure 2B**). The S1 head region of myosin is multifunctional. It contains both the enzymatic ATPase (nucleotide binding) activity which powers the lever arm and the actin-binding domain which forms the crucial actinomyosin complex within the sarcomere.

**B. Contraction in Skeletal Muscle:** An action potential originating in the central nervous system reaches the axon of the motor neuron. This signal activates the voltage-gated calcium channels on the axon so that calcium ions move into the cell. As a result, the intracellular free  $\text{Ca}^{2+}$  concentration increases. This increase causes the acetylcholine vesicles in the axon to fuse with the membrane, releasing the acetylcholine into the synaptic cleft between the motor neuron terminal and the motor end plate of the skeletal muscle fiber (<http://www.wikipedia.org>, 28). The acetylcholine diffuses across the synapse and binds to and activates nicotinic acetylcholine receptor on the motor end plate. Activation of this receptor opens its intrinsic sodium/potassium channel, causing sodium ions to move in and potassium ions to move out. As the channel is more permeable to sodium ions, the muscle fiber membrane becomes more positively charged, triggering an action potential which spreads throughout the muscle fiber and results in the depolarization of the fiber.

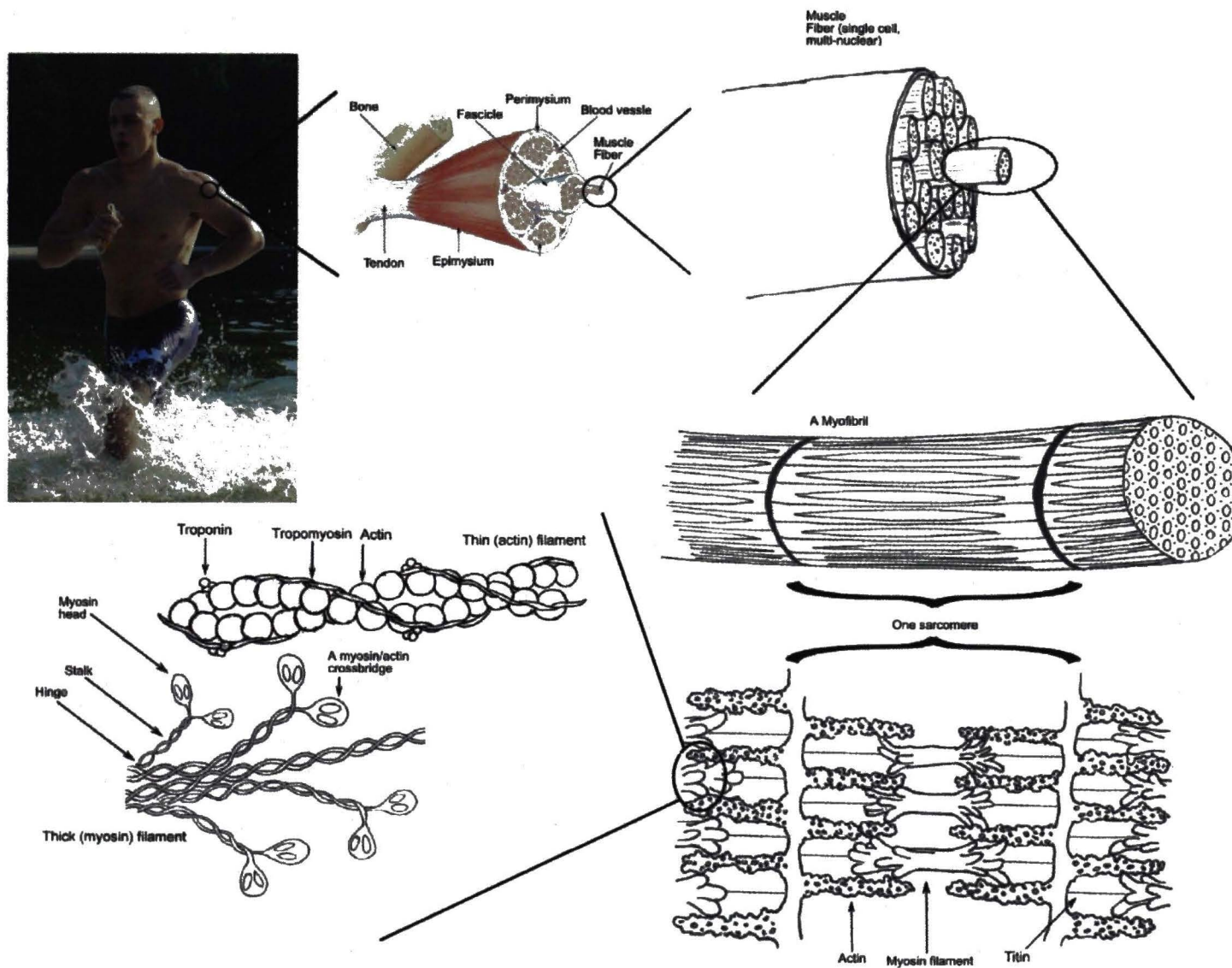


**Figure 1:** Structure of skeletal muscle [http://en.wikipedia.org/wiki/Image:Skeletal\\_muscle.jpg](http://en.wikipedia.org/wiki/Image:Skeletal_muscle.jpg) (GNU Free Documentation).



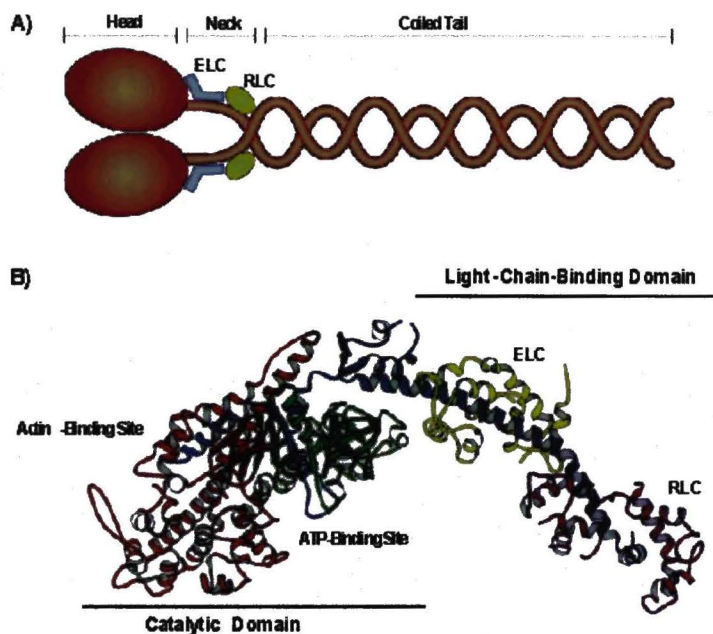


**Figure 2.** A) Schematic representation of a myosin molecule which constitutes the thick filaments of the sarcomere. The myosin molecule is a hexamer consisting of two heavy chains, two essential light chains, and two regulatory light chains. The myosin heavy chains are dimerized through their coiled-coil tails. Reprinted from (61) by permission from MacMillan Publishers, Ltd.

B) Three-dimensional (crystal) structure of a chicken skeletal myosin head (S1). The catalytic and light-chain-binding domains are indicated. The catalytic domain is shown in red, green, and blue. The essential (yellow) and regulatory (purple) light chains wrap around the heavy chain  $\alpha$ -helix (blue). Reprinted from (68) by permission from MacMillan Publishers, Ltd.

The depolarization is detected by the voltage-sensor dihydropyridine receptor coupled to ryanodine receptors on the surface of the sarcoplasmic reticulum. This reaction causes calcium ions to be released from the sarcoplasmic reticulum. After the calcium binds to the troponin present on the thin filaments of the myofibrils, the troponin allosterically modulates the tropomyosin. Normally, the tropomyosin sterically obstructs binding sites for myosin on actin. However, once calcium binds to the troponin, the result is an

allosteric change in the troponin which allows the tropomyosin to dissociate. The binding sites become unblocked, allowing the binding of myosin with actin to occur.

During contraction, the myosin heads attach to actin to form cross-bridges.

Following hydrolysis of ATP, a small conformational change takes place in the myosin catalytic domain. The change is amplified by the neck/regulatory domain, causing the neck region to tilt against the catalytic domain. This tilting action pulls the thin filament towards the center of the sarcomere, resulting in contraction.

**C. Lever arm hypothesis of muscle contraction:** The current hypothesis for the mechanism of force generation by actin-myosin-ATP postulates that the rotation of the lever arm against the catalytic domain is the primary mechanical component of the power stroke (38). The lever arm is a 85Å-stretch of myosin heavy chain, mostly an  $\alpha$ -helix chain, to which the regulatory and essential myosin light chains are bound (**Figure 3**). According to the lever-arm model of muscle contraction, force generation occurs due to the tilting of the regulatory domain against the catalytic domain, causing actin to move 10 nm towards the center of the sarcomere (**Figure 3**) (38).

**D. Cross-Bridge Kinetics:** The cross-bridge cycle has been described as a series of coupled biochemical and mechanical events. The efficient conversion of chemical energy to mechanical energy requires a very precise temporal coupling between the biochemical and mechanical events for which the myosin head is presumed to have been designed. The basic cycle is believed to be the same for all myosins, but the relative rates of the individual steps within each cycle are altered by changes in the amino acid sequence of myosin, which tunes each myosin for its particular physiological role (80). Comparisons

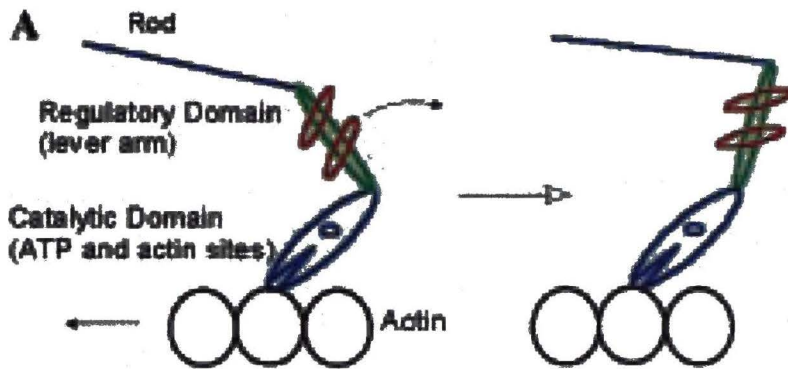


**Figure 3:** Illustration of the rotation of the lever arm against the catalytic domain during force production. Red ellipsoids are RLC and ELC. Reprinted with permission from (38). Copyright (2007), American Chemical Society.

of the properties of different myosins, together with mutagenesis of specific amino acid residues or of short sequences, are the most active areas of current research.  $\tau_1$ ,  $\tau_2$  and  $\tau_3$  are the three primary parameters which affect the cross-bridge kinetics. They are described in detail in the rationale section of this chapter. In the cross-bridge cycle the following major steps are involved (**Figure 4**):

1. ATP dissociates actomyosin into actin and myosin. ATP binds to the myosin head.
2. ATP is hydrolysed. The products ADP (Adenosine diphosphate) and  $P_i$  are bound to myosin. This is the predominant state at rest.
3. Upon muscle stimulation troponin and tropomyosin no longer inhibit actin-myosin interaction. Myosin with ADP and  $P_i$  attaches to actin weakly. It is believed that the angle of cross-bridge attachment is  $90^\circ$ .

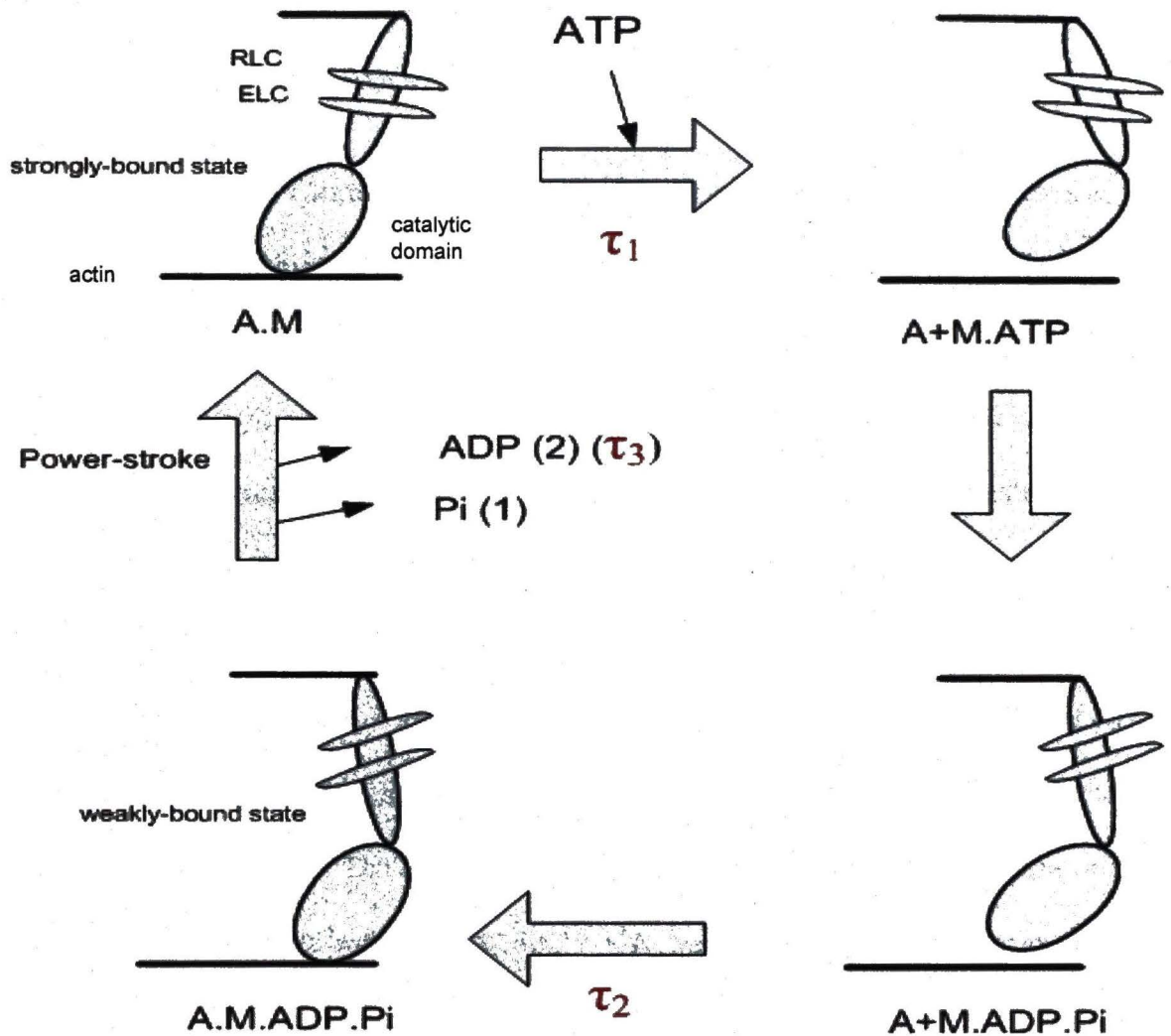


**Figure 4:** Cross-bridge cycle.  $\tau_1$  is the dissociation time of myosin heads (M) from actin (A),  $\tau_2$  is the rebinding time of cross-bridges to actin; and  $\tau_3$  is the dissociation time of ADP from the active site of myosin. Adapted from (31) with permission from MacMillan Publishers, Ltd.

4. The actin-myosin interaction triggers the sequential release of  $P_i$  and ADP from the myosin head, resulting in the power stroke. It is proposed that the conformational change in the cross-bridge tilts the angle of the cross-bridge attachment from  $90^\circ$  to  $45^\circ$ . It is currently believed that the regulatory domain of



myosin acts as a “lever arm” which amplifies the small conformational changes of the myosin head. This tilting pulls the actin filament about 10 nm toward the center of the sarcomere by utilizing the energy stored in myosin.

**E. Regulatory Light Chain:** There is substantial evidence that myosin RLC plays a primary regulatory role in scallop and smooth muscle contractions, but its functional role in mammalian striated (skeletal and cardiac) muscle contraction is unclear (87). RLC, together with the ELC, stabilizes the 8.5 nm-long  $\alpha$ -helical neck region of the myosin head, with the N-terminus of RLC wrapped around the heavy chain. These calmodulin-like light chains are non-covalently bound to the heavy chain of myosin, with RLC arranged such that its N-terminal domain wraps around the C-terminus of the heavy chain in the region between Glu 808 and Val 826 (69). The structure of the N-terminus of RLC is similar to other  $\text{Ca}^{2+}$  binding proteins such as calmodulin, troponin, and ELC, while the C-terminus is less similar. The N-terminus domain of the RLC contains a divalent cation-binding site, which binds both  $\text{Ca}^{2+}$  and  $\text{Mg}^{2+}$ . It is thought that this site is occupied by  $\text{Mg}^{2+}$  and may become saturated with  $\text{Ca}^{2+}$  in relaxed muscle, depending on the length of the  $\text{Ca}^{2+}$  concentration transient. Similar to smooth muscle myosin, the N-terminal domain of RLC of skeletal and cardiac myosins contains a phosphorylation site (Serine) that is located in proximity to the cation-binding site.

**F. Effect of RLC Phosphorylation and  $\text{Ca}^{2+}$  Binding in Skeletal Muscle Contraction**  
During skeletal muscle contraction, the increase in intracellular  $\text{Ca}^{2+}$  concentration activates the  $\text{Ca}^{2+}$ /Calmodulin-dependent myosin light chain kinase (MLCK) and leads to phosphorylation of RLC. There have been numerous studies with contradictory results

with regard to the effect of phosphorylation of the RLC on skeletal muscle contraction. *In-vivo* studies with intact skeletal muscle have demonstrated that the level of myosin phosphorylation significantly increases after tetanic stimulation (55). RLC phosphorylation in skinned-muscle fibers has a small effect on the  $\text{Ca}^{2+}$  sensitivity of isometric tension, whereas it has a significant effect on the rate of force redevelopment (55, 85). On the other hand, several studies have suggested that phosphorylation of the RLC reduces cross-bridge cycling rates (20, 21). However, *in-vitro* experiments found no evidence correlating phosphorylation of the RLC with skeletal muscle regulation (17).

There are also contradictory reports as to whether the phosphorylation influences actin-activated myosin ATPase activity (66, 83). Recent studies by Szczesna et al. (90) have demonstrated that phosphorylation of the RLC by  $\text{Ca}^{2+}$ /calmodulin-activated MLCK has a significant effect on the maximal development of  $\text{Ca}^{2+}$  sensitivity of force in skinned skeletal muscle fibers and on the ATPase activity in reconstituted thin filaments. A shift towards lower  $\text{Ca}^{2+}$  concentrations in the actin-tropomyosin-troponin-activated myosin ATPase activity was observed for the phosphorylated-RLC reconstituted myosin but not for the non-phosphorylated RLC. Using skinned skeletal muscle fibers resulted in a 15% increase in maximal force developed by phosphorylated-RLC skinned fibers but not for those fibers reconstituted with non-phosphorylated RLC. Consistent with previous studies (55, 85), Szczesna et al. showed that the force-pCa relationship shifts towards lower concentrations of  $\text{Ca}^{2+}$  as a result of RLC phosphorylation. In summary, although some recent studies have demonstrated that RLC modulates muscle contraction through

maximal force development, the role of RLC phosphorylation in striated muscle contraction is still not clear.

### **G. Modulation of Skeletal Muscle Contraction by RLC Phosphorylation and $\text{Ca}^{2+}$**

**Binding:** The relationship between phosphorylation of RLC and its  $\text{Ca}^{2+}$ -binding site is still under investigation. The work by Szczesna et al. (90) in skeletal muscle suggests that the  $\text{Ca}^{2+}$ -binding site and the phosphorylation site (Ser-15) communicate with each other and that this intramolecular communication is important for the phosphorylation-dependent effects on force generation (including alteration in  $\text{Ca}^{2+}$  sensitivity and maximal force) (**Figure 5**). At the molecular level, the phosphorylation-dependent force potentiation may simply result from the recruitment of more strongly bound cross-bridges as the phosphorylation of the RLC causes cross-bridges to move away from the thick filament backbone and become more accessible to actin (85) (**Figure 5**). This potentiation was illustrated by electron micrographs of permeabilized rabbit psoas fibers containing phosphorylated thick filaments, whose near-helical periodic arrangement (characteristic of the relaxed state) was lost due to RLC phosphorylation (101). It is possible that the change in charge at the N-terminus, produced by RLC phosphorylation, increases the myosin head mobility and the ordered array of myosin heads on actin filaments observed under relaxed conditions (49). According to Davis et al. (22), RLC phosphorylation may increase the number of cross-bridges entering the contractile cycle by up-regulation of actin-induced phosphate release. RLC phosphorylation could regulate the transition from the "**actin-S1.ADP.P1**" to the "**actin-S1.ADP**" state (**Figure 5**) and thus modulating the cross-bridge cycle. In summary, recent studies support the contention



that the  $\text{Ca}^{2+}$ -binding site is important for the RLC phosphorylation-mediated effects on muscle contraction.

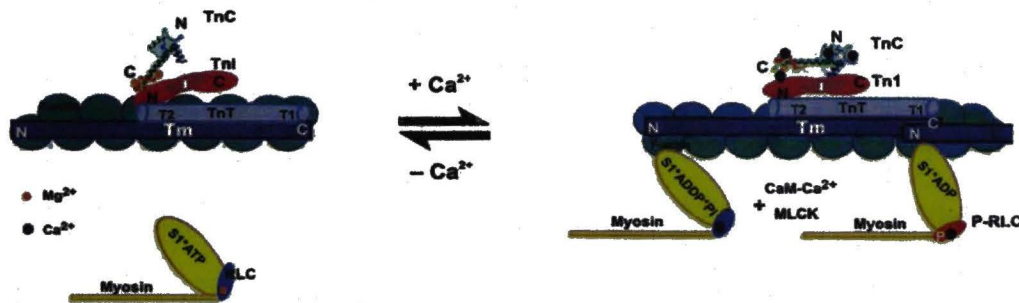


**Figure 5:** Illustration of  $\text{Ca}^{2+}$ -troponin-tropomyosin-regulated striated muscle contraction and the effect of RLC phosphorylation and  $\text{Ca}^{2+}$  binding. Repetitive stimulation of the striated muscle elevates the intracellular  $\text{Ca}^{2+}$  level, which in turn activates the  $\text{Ca}^{2+}$ -Calmodulin-dependent-MLCK complex and leads to RLC phosphorylation (89). (Copyright permission granted from Bentham Publishers)

## 2. Structure and Function of Cardiac Muscle

**A. Structure:** Cardiac muscle resembles skeletal muscle in that it is striated and multinucleate. Skeletal and cardiac muscle are called striated muscles. Cardiac muscle fibers are comprised of separate cellular units (myocytes) connected in a series. In contrast to skeletal muscle fibers, cardiac muscle fibers do not assemble in parallel arrays but bifurcate and recombine to form a complex three-dimensional network and have centrally rather than peripherally positioned nuclei. Cardiac muscle contains **intercalated discs**, which allow communication between adjacent cells such that there is a sequential contraction of the cells from the apex of the ventricle to the base, facilitating maximal ejection of blood from the ventricle during contraction. This occurs without nerve innervations to each cell or group of cells. The structure of the cardiac sarcomere is very



similar to the skeletal myosin (**Figure 6**). There are two isoforms of cardiac MyHC,  $\alpha$  and  $\beta$ , which dimerize to form  $\alpha\alpha$  (V1),  $\beta\beta$  (V2), and  $\alpha\beta$  (V3) isozymes. The dominant myosin isozyme of the left ventricle is  $\alpha$ -MyHC in rodents and  $\beta$ -MyHC in humans. The  $\alpha$ - and  $\beta$ - chains are 93% homologous but have different rates of ATP hydrolysis, with the  $\alpha\alpha$  isoform having a faster rate of ATP hydrolysis than the  $\beta\beta$  isoform (72). Since cardiac myocytes contain either predominantly fast  $\alpha\alpha$  (as in a mouse ventricle) or slow  $\beta\beta$  (as in a human ventricle) myosin, the intrinsic ATPase activities of the myosin ATPase isozymes account for the differences in the shortening velocities of the cardiac muscles of different species.

**B. Contraction:** Heart contraction is initiated through action potentials, though in a different manner than skeletal muscle contraction. Skeletal muscle contraction is initiated by electrical impulses from motor nerve terminals located on individual muscle fibers. Heart cells, however, have no motor nerve terminals attached to them, and their contraction can occur without an initial nervous input. The cells which produce stimulation for contraction without nervous input are called pacemaker cells which communicate with each other directly by passing electrical impulses to neighboring cells through special channels called **gap-junctions/intercalated discs**. This process allows the heart to be stimulated at only one location as the electrical impulse passes on to the rest of the heart muscle, resulting in contraction. Once the action potential is triggered, the mechanism of cardiac muscle contraction is similar to that of skeletal muscle contraction.

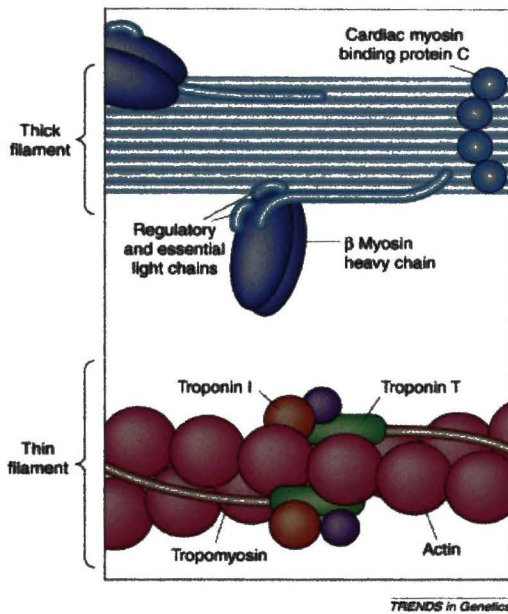


**Figure 6:** The cardiac sarcomere comprise the contractile proteins of the thick and thin filaments. Reprinted from (5) with permission from Elsevier.

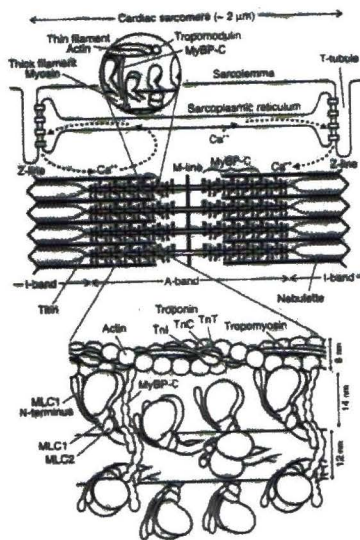


**Figure 7:** Cardiac sarcomere in relation to the membranous structures responsible for intracellular Ca<sup>2+</sup> handling. Adapted from (54). Reprinted with kind permission from Springer Science and Business Media.

### C. Role of $\text{Ca}^{2+}$ in Cardiac Muscle Contraction and Cross-Bridge Kinetics:

The importance of  $\text{Ca}^{2+}$  in the regulation of contraction in normal myocytes and in cardiomyopathies has increasingly been recognized. The intracellular free  $\text{Ca}^{2+}$  concentration ( $[\text{Ca}^{2+}]_i$ ) is critical in muscle contraction and relaxation regulation. Muscle contraction is initiated by an increase in  $[\text{Ca}^{2+}]_i$  which results from the depolarization-induced influx of a small amount of  $\text{Ca}^{2+}$  via voltage-gated dihydropyridine receptors in T-tubules. This process triggers the release of a large quantum of  $\text{Ca}^{2+}$  from the sarcoplasmic reticulum (**Figure 7**). The increase in  $[\text{Ca}^{2+}]_i$  promotes  $\text{Ca}^{2+}$  binding to multiple buffers, including troponin C. The troponin-tropomyosin complex acts as a  $\text{Ca}^{2+}$ -sensitive switch which regulates actin-myosin interaction (28). During diastole, the binding of troponin to actin-tropomyosin inhibits actin-myosin interaction.  $\text{Ca}^{2+}$  binding to troponin C induces a conformational change which weakens the interaction between troponin I and actin-tropomyosin and strengthens the interaction between troponin I and troponin C (28). These changes release the thin filament from its inhibitory state, promoting actin-myosin interaction and force generation.

Earlier studies have reported a  $\text{Ca}^{2+}$ -dependent rate of force development in striated muscle (4). However, the mechanism responsible for the  $\text{Ca}^{2+}$  dependence on the rate and extent of force development in cardiac muscle was not clear. Brenner (15) showed that  $\text{Ca}^{2+}$  accelerates cross-bridge kinetics in skeletal muscle when measured by the rate of force redevelopment after forcible detachment of the cross-bridges during  $\text{Ca}^{2+}$  activation. He therefore proposed a kinetic model in which  $\text{Ca}^{2+}$  activates both force and rate of force redevelopment by increasing the rate of transition of cross-bridges from the



non-force-generating (detached- or weakly-bound) state to the force-generating state. A recent study using laser photolysis indicated that the power stroke, or the force-generating step, in the cross-bridge cycle of cardiac muscle is sensitive to  $[Ca^{2+}]_i$ . This suggests that the  $Ca^{2+}$  controls the attachment step in the cross-bridge cycle via a rapid equilibrium with the thin filament activation state (53).

#### **D. Effect of RLC Phosphorylation and $Ca^{2+}$ Binding in Cardiac Muscle**

**Contraction:** The ventricular-myosin RLC is expressed both in the ventricular myocardium and in the slow-twitch skeletal muscle. Phosphorylation of RLC increases the submaximal isometric tension, inducing a leftward shift in the tension-pCa curve and increasing the rate of force development (55) but not changing the maximal isometric tension (67). Replacement of the phosphorylatable serines (Ser 14, 15, and 19) with alanines in mouse ventricular RLC induces a variety of negative cardiovascular changes in transgenic mice, such as reduced cardiac output (71, 74).

The importance of ventricular RLC for normal mammalian cardiac function is demonstrated by its correlation with human diseases. Phosphorylation of ventricular RLC is decreased in heart-failure patients as well as in diabetic-cardiomyopathic rats (59). In contrast, RLC phosphorylation is elevated in rats during increased beat frequency or increased left-ventricular pressure due to exercise or inotropic agents (29). In another study, the effect of RLC phosphorylation on cardiac mechanics was studied on the slow fibers from rabbit soleus muscles (22). These fibers are appropriate for study because both human and rabbit slow-skeletal muscle express the ventricular myosin RLC isoform. A dramatic 2.5-fold increase in isometric tension caused by RLC phosphorylation was



monitored in slow muscle fibers (22). Because the contracting heart works at half the maximum  $\text{Ca}^{2+}$  activation, RLC phosphorylation could be modulating cardiac contraction from low tension to full power at a fixed concentration of  $\text{Ca}^{2+}$ .

### **3. Familial Hypertrophic Cardiomyopathy**

Familial Hypertrophic Cardiomyopathy (FHC) is a relatively common primary cardiac disorder defined as the presence of a hypertrophied left ventricle in the absence of any other diagnosed etiology (93). The prevalence of FHC in the general population is 0.2% (or 1 in 500). Patients with FHC show remarkable diversity in clinical presentations, ranging from no symptoms to severe heart failure and sudden cardiac death (93). The disease is transmitted as an autosomal dominant trait such that the offspring of affected individuals have a 50% chance of inheriting the gene mutation.

#### **A. Genetic Analyses and Diagnosis of Familial Hypertrophic Cardiomyopathy:**

Molecular genetic studies have shown that at least 11 different genes are currently known to cause FHC. Ten of these 11 genes, including the cardiac  $\beta$ -myosin heavy chain, the ventricular myosin ELC, the ventricular myosin RLC, cardiac troponins,  $\alpha$ -tropomyosin, myosin binding protein C, and titin and actin genes, encode for sarcomeric proteins (**Table 1**) (97, 68). The relative frequency of these causative sarcomeric genes in FHC is summarized in Table 1. More than 200 mutations have been identified so far in these genes, with most being of the missense type (i.e., a single base change resulting in an amino acid substitution). Although much is known about which genes cause disease,

relatively little is known about the molecular steps leading from the gene defect to the clinical phenotype and what factors modify the expression of mutant genes.

**Table 1.** Sarcomeric Proteins and Genes Responsible for FHC. Adapted from (68).

Sarcomeric protein	Frequency	Number of mutations
$\beta$ -Myosin heavy chain	~ 30%	70
Myosin binding protein-C	~ 20%	29
Cardiac troponin T	~ 20%	14
$\alpha$ -Tropomyosin	~ 5%	4
Cardiac troponin I	~ 5%	8
Regulatory light chain	1 – 7%	11
Essential light chain	~ 1%	3

The minimum investigative process required for the diagnosis of FHC includes an electrocardiogram (ECG) and a transthoracic echo Doppler examination. The ECG is generally abnormal in FHC patients, although entirely normal ECGs are seen in about 15% of patients (which are usually found in the presence of only localized left-ventricular hypertrophy) (44). The most common abnormalities are left ventricular hypertrophy, negative T-waves, ST abnormalities, and pathological Q-waves (44). All these abnormalities are usually absent in children and become evident over time with the development of left ventricular hypertrophy. However, in some cases, especially in the young, ECG may be abnormal, even when an echocardiography reveals no left-ventricular hypertrophy. Transthoracic echo Doppler examination is the most important diagnostic test in FHC. The ECG and transthoracic echo Doppler examination are used to assess the extent and distribution of hypertrophy, systolic and diastolic function, presence of systolic anterior motion of the mitral valve, and severity of the pressure gradient (44).

## B. RLC Mutations Associated With Familial Hypertrophic Cardiomyopathy:

Recent studies have revealed that the ventricular isoform of myosin RLC is one of the sarcomeric proteins associated with FHC. To date 10 RLC mutations identified in North American, European, and South African populations have been linked to FHC (**Figure 8A**). Some of these mutations (A13T, E22K, and P95A) have been shown to be associated with a particular subtype of FHC defined by mid-left-ventricular obstruction (67). Other mutations (F18L, N47K, R58Q, K104E, and D166V) result in a more classic form of FHC which results in increased left-ventricular wall thickness and abnormal ECG (2, 30, 44, 70). The RLC mutations R58Q and D166V have been associated with a malignant disease phenotype and sudden cardiac death (44, 70).

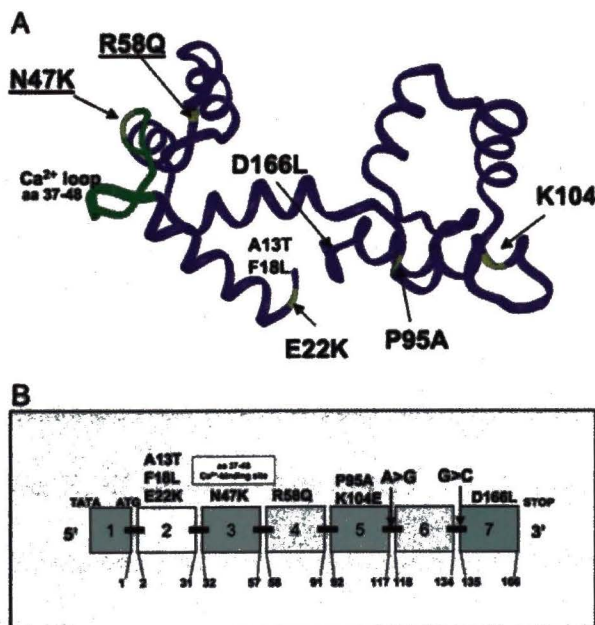


**Figure 8:** A) three-dimensional representation of human cardiac RLC (HCRLC). FHC mutations and the Ca<sup>2+</sup> binding site are labeled. B) Exon organization of HCRLC and the sites of all FHC mutations identified to date (91). (JBC grants use without copyright permission)



**C. Experimental Systems Utilized to Study FHC-RLC Mutations:** A number of experimental systems have been successfully employed to study FHC-RLC mutations. These include binding assays, in-vitro motility assays using bacterially-expressed and -purified RLC, reconstitution experiments, exchange of mutant RLC into skinned myofibers, and studies with transgenic (Tg) mice.

**(i) Studies with Bacterially Expressed and Purified Human Cardiac RLC and Its**

**FHC Mutants:** The effect of FHC mutations on RLC-phosphorylation,  $\text{Ca}^{2+}$ -binding properties, and secondary structure was studied by Szczesna et al. (87). The three-dimensional structure of the RLC demonstrates the close proximity of FHC mutations to either the Ser-15 phosphorylation site of RLC (A13T, F18L, E22K) or the  $\text{Ca}^{2+}$ -binding loop between the amino acids 37 and 48 (E22K, N47K, R58Q) (**Figure 8A**).

The  $\text{Ca}^{2+}$ -binding properties of human cardiac RLC (HCRLC) and five recombinant RLC-FHC mutants were tested with the flow-dialysis method (87, 91, 75). Three of the FHC mutations—A13T, F18L, and P95A—decreased the calcium binding affinity ( $K_{\text{Ca}}$ ) by 3-fold, whereas three other mutations—E22K, N47K and R58Q—changed the  $\text{Ca}^{2+}$ -binding properties in a more drastic manner. Compared with Wild-type (WT)-HCRLC, the E22K mutation decreased the  $K_{\text{Ca}}$  value by approximately 17-fold, whereas the R58Q and N47K mutant showed no  $\text{Ca}^{2+}$ -binding (**Table 2**). Phosphorylation of WT with  $\text{Ca}^{2+}$ -calmodulin activated MLCK decreased its  $\text{Ca}^{2+}$ -binding affinity by 7-fold.

However, the effect of FHC mutations on the  $\text{Ca}^{2+}$  properties of HCRLC varied depending upon the location of the mutation (**Table 2**). The most dramatic effect was



observed for the E22K mutant. This substitution prevented the E22K mutant from being phosphorylated; even a 20-fold increase in the enzyme/substrate ratio and longer incubation time did not result in phosphorylated E22K. A great effect from phosphorylation was also observed for the A13T mutation. Phosphorylation of A13T resulted in a large increase in its  $\text{Ca}^{2+}$ -binding affinity compared with phosphorylation of non-phosphorylated A13T. Phosphorylated A13T demonstrated a 15-fold greater affinity for  $\text{Ca}^{2+}$  than non-phosphorylated WT. Phosphorylation produced no observable effects on  $\text{Ca}^{2+}$  binding to F18L. However, phosphorylation resulted in an interesting effect on  $\text{Ca}^{2+}$  binding to the R58Q mutant; this mutant did not bind  $\text{Ca}^{2+}$  in the non-phosphorylated state but did bind  $\text{Ca}^{2+}$  when phosphorylated.

**Table 2** shows that the A13T and E22K FHC mutants had significantly increased  $\alpha$ -helical contents in apo-state (metal free) when monitored by UV-CD (Circular Dichroism) spectroscopy (88). All the other FHC mutants did not alter the  $\alpha$ -helical content in the apo-state.  $\text{Ca}^{2+}$  binding resulted in an increased  $\alpha$ -helical content in both HCRLC-WT and P95A (88). Interestingly, the binding of  $\text{Ca}^{2+}$  to the A13T mutant, which had the highest  $\alpha$ -helical content among all the FHC mutants in the apo-state, caused a decrease in its  $\alpha$ -helical content from 29% to 25%. However, the amount of  $\alpha$ -helical content of the  $\text{Ca}^{2+}$ -bound A13T was the same as for the other  $\text{Ca}^{2+}$ -bound mutants. The  $\alpha$ -helical content of the A13T mutant returned to a normal level (that of WT) upon phosphorylation. Therefore, phosphorylation of the A13T mutant attenuated whatever sterical constraints were introduced by this FHC mutation. Another interesting effect of phosphorylation on  $\text{Ca}^{2+}$  binding was observed for the R58Q mutant. This

mutant could not bind  $\text{Ca}^{2+}$  in the non-phosphorylated state but could bind  $\text{Ca}^{2+}$  after phosphorylation. The FHC-RLC mutations either reduced or eliminated  $\text{Ca}^{2+}$  binding in the non-phosphorylated state. However, upon phosphorylation depending on the type of mutation phosphorylation either restored  $\text{Ca}^{2+}$  binding or the FHC-RLC mutant could not be phosphorylated

**Table 2.** Effect of FHC Mutations and Phosphorylation on  $\text{Ca}^{2+}$  Binding to Human Cardiac RLC (88, 92). (ND-Not determined)

Protein	$K_{\text{Ca}}$ ( $\text{M}^{-1}$ )		$\alpha$ -Helical Content			
	Nonphosphorylated	Phosphorylated (Ser-15)	Apo	+ $\text{Ca}^{2+}$	+P	+P+ $\text{Ca}^{2+}$
HCRLC-WT	$6.67 \pm 0.21 \times 10^5$	$0.90 \pm 0.06 \times 10^5$	18%	23	18	18
A13T	$2.06 \pm 0.23 \times 10^5$	$13.27 \pm 0.24 \times 10^5$	29	25	19	18
F18L	$2.38 \pm 0.25 \times 10^5$	$3.58 \pm 0.88 \times 10^5$	22	24	22	21
E22K	$0.39 \pm 0.09 \times 10^5$	No phosphorylation	24	20	No P	No P
R58Q	No binding	$3.04 \pm 1.02 \times 10^5$	20	22	20	28
P95A	$2.11 \pm 0.77 \times 10^5$	ND	19	23	ND	ND
N47K	No binding	ND	19	ND	ND	ND

**In summary,** the studies described above reveal the effect of FHC-RLC mutations on phosphorylation,  $\text{Ca}^{2+}$  binding, and RLC secondary structure.  $\text{Ca}^{2+}$  binding was restored to R58Q upon phosphorylation, E22K experienced decreased  $\text{Ca}^{2+}$  affinity and could not be phosphorylated,  $\text{Ca}^{2+}$  binding to E22K and A13T decreased the  $\alpha$ -helical content

which had been initially increased by the FHC mutation, and phosphorylation of A13T restored the amount of  $\alpha$ -helical content to the level of wild-type.

**(ii) Studies with Reconstituted Muscle Preparations:** In reconstituted muscle preparations, the mutant RLC is introduced into normal muscle fibers so that the effects observed are directly related to the function of myosin and are not complicated by the slowly-developing secondary effects often observed with cardiac tissue from diseased patients or transgenic animals (e.g., cellular disarray, fibrosis, and hypertrophy). Another advantage of this *in-vitro* study is that the amount of mutant RLC in the muscle fiber could be quantitated by gel electrophoresis, whereas diseased human tissue most likely contains a mixture of mutant and normal ventricular RLC (71).

Roopnarine (71) studied the effect of A13T, F18L, E22K, and P95A in ventricular RLC on force generation as a function of  $\text{Ca}^{2+}$  concentration. The endogenous RLC was extracted from skinned rabbit psoas muscle fibers reconstituted with either rat WT ventricular RLC (vRLC) or recombinant vRLC (A13T, F18L, E22K and P95A). Compared to fibers from wild-type rat ventricular RLC (vRLC), the fibers with E22K-RLC mutant demonstrated increased  $\text{Ca}^{2+}$  sensitivity of force generation above 10% of maximal tension, whereas the fibers from A13T-RLC and F18L-RLC mutants demonstrated decreased  $\text{Ca}^{2+}$  sensitivity, and the P95A-RLC mutant demonstrated no significant effect (**Table 3**). With the exception of F18L, none of the RLC mutants decreased the maximal tension at saturating  $\text{Ca}^{2+}$  conditions, which decreased the maximal tension to 70% of the wild-type value. These results suggest that the primary cause of FHC in these mutants is perturbation in the calcium sensitivity of force



generation such that  $\text{Ca}^{2+}$ -sensitizing or  $\text{Ca}^{2+}$ -desensitizing effects can lead to similar disease phenotypes. Szczesna et al. (91) investigated the functional effects of A13T, F18L, E22K, N47K, R58Q, and P95A mutations on  $\text{Ca}^{2+}$  sensitivity of force/ATPase when reconstituted in skinned porcine cardiac muscle preparations. These muscle systems provide important physiological information, such as myofibrillar ATPase activity, steady-state force development, and  $\text{Ca}^{2+}$  sensitivity of ATPase/force (**Table 3**). The  $\text{Ca}^{2+}$  sensitivity of myofibrillar ATPase activity was significantly increased for the N47K mutant and only slightly increased for the E22K and R58Q mutants. The reconstituted muscle fibers were also tested for steady-state force development and the regulation of  $\text{Ca}^{2+}$  sensitivity of force. Reconstitution with the E22K, N47K, and R58Q mutants significantly reduced steady-state force. N47K and R58Q RLC reconstituted myofibrils showed an increase in the  $\text{Ca}^{2+}$  sensitivity of force, with R58Q myofibrils demonstrating a significantly higher  $\text{Ca}^{2+}$  sensitivity of force than N47K microfibrils.

**In summary**, both studies (71, 91) revealed observable effects of FHC-RLC mutations on reconstituted muscle preparations. Roopnarine (71) used rabbit psoas muscle fibers reconstituted with rat ventricular RLC with the FHC mutations inserted into the amino acid positions homologous to human ventricular RLC. Szczesna et al. (91) used porcine papillary muscle fibers reconstituted with human ventricular RLCs. Both studies found that the E22K mutation increased  $\text{Ca}^{2+}$  sensitivity of force. However, Szczesna et al. did not observe dramatic changes in the maximal isometric tension and calcium sensitivity of force generated by the F18L mutation. This discrepancy could be due to the fact that Roopnarine et al. used skeletal fibers whereas Szczesna et al. used



cardiac fibers. Roopnarine et al. were able to extract 50% of the endogenous RLC from skeletal fibers, whereas Szczesna et al. were able to extract 80-90% of endogenous RLCs from cardiac fibers. Roopnarine observed the effects of force development partially produced by skeletal RLC and partially produced by cardiac RLC. These two different RLC isoforms could generate different fiber kinetics, force development, and  $\text{Ca}^{2+}$  sensitivity. According to an earlier study (32) the replacement of cardiac RLC with fast-skeletal muscle RLC isoform reduces left-ventricular contractility and relaxation.

**Table 3:** Effect of FHC-RLC Mutations on Mechanical Properties in Reconstituted Muscle Preparations. (ND—Not determined)

FHC	Roopnarine, (2003) (71) Rabbit psoas muscle fiber reconstituted with rat WT or recombinant rat vRLC		Szczesna et al., (2004) (91) Porcine cardiac muscle preparations reconstituted with WT- human cardiac RLC or its FHC mutants (A13T, F18L, E22K, N47K, R58Q, P95A)			
	$\text{Ca}^{2+}$ sensitivity of force generation	Maximal tension at saturating $\text{Ca}^{2+}$ concn	Myofibrillar ATPase activity	$\text{Ca}^{2+}$ sensitivity of ATPase	Steady state force	$\text{Ca}^{2+}$ sensitivity of force
A13T	decreased	No effect	No effect	No effect	No effect	No effect
F18L	decreased	decreased	No effect	No effect	No effect	No effect
E22K	Increased	No effect	No effect	Increased	Decreased	Increased
P95A	No effect	No effect	No effect	No effect	No effect	No effect
N47K	ND	ND	No effect	Increased	Decreased	Increased
R58Q	ND	ND	No effect	Increased	Decreased	Increased

**Overall**, the largest effect on the mechanical properties of reconstituted muscle preparations was seen for the three FHC mutations E22K, N47K, and R58Q, which are located directly in or near the single  $\text{Ca}^{2+}$ - $\text{Mg}^{2+}$ -binding site of HCRLC. When reconstituted in porcine cardiac muscle preparations, these three mutants increased the

$\text{Ca}^{2+}$  sensitivity of myofibrillar ATPase activity and the steady-state force (**Table 3**). All three of these mutants have shown significantly reduced or no  $\text{Ca}^{2+}$  binding in the flow dialysis studies with bacterially-expressed and purified human cardiac RLC and its FHC mutants (**Table 2**). These results suggest the importance of the intact  $\text{Ca}^{2+}$ -binding site of HCRLC in the regulation of cardiac muscle contraction and its possible role in the RLC-linked pathogenesis of FHC.

**(iii) Studies with Transgenic Mice and Other Animal Models:** A number of transgenic animals have been produced to express a variety of mutant cardiac sarcomeric proteins. Studies in humans are limited because of factors including variable genetic backgrounds, environmental stimuli which may differ between individuals (i.e., exercise and lifestyle), a limited number of individuals with the same mutation, the relative difficulty in obtaining human cardiac samples, and inadequate methods of maintaining human-heart tissue in cell-culture systems (97). Transgenic animal production has been particularly useful in studying FHC because it provides an unlimited supply of "patients" with the same mutation maintained in a controlled environment who can provide unlimited tissue samples (97). Animal models are also very useful because stable cell lines of myocyte lineages do not exist. Genetically engineered mice which express human FHC mutations have been particularly useful. The usefulness of these animal models has been substantially increased by the miniaturization of many diagnostic procedures used to evaluate cardiac function in humans. For example, exercise protocols and provocative electrophysiological testing in mice can evaluate the role of vigorous exercise in sudden death and FHC.

Human mutations in MyHC (33), myosin-binding protein C (102), and troponin (93) have been genetically engineered into genomes of mice and rabbits (52). These animal models exhibit many characteristics of the human disease, including cardiac hypertrophy and such histopathological features of myocyte disarray as increased interstitial fibrosis and altered cardiac physiology (76). Most recently, a bigenic (two-gene) model of FHC has been developed, allowing the mutant troponin gene to be turned "on" or "off" using a ligand-inducible system (51).

The first and most extensively studied mouse model (Arg403Gln mutation in Myosin Heavy Chain) illustrates how the human disease is replicated in mice. Introducing an Arg403Gln mutation in the  $\alpha$ -cardiac myosin heavy chain gene by gene-targeting and homologous recombination generated this mouse model (34). This mutation is well characterized in humans with FHC and is associated with high penetrance (> 90% express the phenotype by age 20) and early sudden death. In brief, Arg403Gln mice develop histopathological changes of FHC (myocyte hypertrophy, disarray, and fibrosis) by the age of 15 weeks and echocardiographically detectable hypertrophy by 30 weeks. These animal models of human FHC thus provide evidence that a mutation in a sarcomeric gene is indeed the primary cause of FHC. Recently, transgenic rabbits expressing FHC-causing mutations have been generated which can be used to further study FHC.

There are some fundamental differences between the human heart and the mouse heart. In particular, the type of motor protein is different;  $\beta$ -MyHC is the predominant myosin isoform in the human heart, whereas  $\alpha$ -MyHC is the predominant myosin

isoform in the mouse heart. The mouse heart beats ten times faster than the human heart. As a result, the cardiovascular outcomes of transgenic mice produced with FHC mutations must not be assumed to be the outcomes for human hearts.

Compared to the mouse heart, the rabbit heart is more closely related to the human heart at the molecular, biochemical, and physiological levels. Similar to human hearts, rabbit hearts express the “slow”  $\beta$ -MHC myosin isoform. Compared to mouse hearts, rabbit hearts are larger and have a slower contraction rate. These attributes are advantageous for physiological analyses such as echocardiography. The transgenic rabbit model expressing Arg403Gln-MHC mutation exhibits a phenotype virtually identical to human FHC (52).

Szczsna-Cordary et al. (88) have generated transgenic mice that overexpress human cardiac E22K-RLC in the murine heart. The expression of myc-E22K occurs under the control of the murine  $\alpha$ -myosin heavy chain promoter. The researchers used hearts from nine-month old and 13-month old mice. In both cases, the hearts of Tg-E22K mice demonstrated visibly enlarged inter-ventricular septa and papillary muscles. These results suggest that the human phenotype of the E22K-mutated hearts (44, 68) could be reproduced in transgenic mice. There were no differences in heart weight to body weight ratios in mice expressing E22K mutation. However, the echocardiographic abnormalities observed in most of the human patients with the E22K mutation were not detected in these transgenic mice. At present it is not known why the differences which appear in the histopathology images are not supported by echocardiography results. Perhaps the use of



a new echocardiogram technology developed for small animals could capture the differences in systole and diastole.

Sanbe et al. (74) have also generated transgenic mice expressing the E22K-RLC mutation. The transgenic mice generated by Sanbe's group express murine RLC isoform, unlike the transgenic mice developed by Szczsna-Cordary's group which express human RLC isoform. The amino acid similarity between human vRLC and mice vRLC is 95%, with 100% similarity in the amino acids flanking the E22K-FHC mutation (**Figure 9**). Therefore, the murine vRLC is a good model for studying the FHC mutations. Unlike the murine model carrying the human RLC gene-locus generated by Szczsna-Cordary's group, mice with the mutated murine RLC generated by Sanbe's group failed to exhibit overt hypertrophy or mid-ventricular cavity obstruction. Since the major focus of Sanbe et al.'s study was the essential light chain of myosin, no functional examination was performed on their E22K-RLC transgenic mice.

RLC		A13T	S15	F18L	E22K	Ca <sup>2+</sup> -binding loop	
Human Ventricular	APKKAKKRAGG	AN	-----	SNVFSMF	Q	QIQEFKEAFTIMDQNRDGFIDKNDLRDTFAAL	55
Mouse Ventricular	APLFAKKRIEG	GT	-----	SNVFSMF	Q	QIQEFKEAFTIMDQNRDGFIDKNDLRDTFAAL	55
Rat Ventricular	SPKAKKRLEG	GS	-----	SNVFSMF	Q	QIQEFKEAFTIMDQNRDGFIDKNDLRDTFAAL	55
Chicken Cardiac A	APKKAKKRIEG	AN	-----	SNVFSMF	Q	QIQEFKEAFTIMDQNRDGFIDKADLRDTFAAL	55
Chicken Cardiac B	-PKKAKKVEG	Q	-----	SNVFSMF	Q	QIQEFKEAFTIMDQNRDGFIDKADLRDTFAAL	53
Rabbit Skeletal	APKKAKKRAA	EGGS	---	SNVFSMF	Q	QIQEFKEAFTVIDQNRDGIIDKEDLRDTFAAM	57

RLC		R58Q	P95A	
Human Ventricular	GLNVVKNEEIDEMIK	EAPGPINFTVFLTMFGEKLGADFEETILNAFKVFDPEGKGLKA	115	
Mouse Ventricular	GLNVVKNEEIDEMIK	EAPGPINFTVFLTMFGEKLGADFEETILNAFKVFDPEGKGLKA	115	
Rat Ventricular	GLNVVKNEEIDEMIK	EAPGPINFTVFLTMFGEKLGADFEETILNAFKVFDPEGKGLKA	115	
Chicken Cardiac A	GLNVVKNEEIDEMIK	EAPGPINFTVFLTMFGEKLGADFEETILNAFKVFDPEGKGLKA	114	
Chicken Cardiac B	GLNVVKNEEIDEMIK	EAPGPINFTVFLTMFGEKLGADFEETILNAFKVFDPEGKGLKA	113	
Rabbit Skeletal	GLNVVKNEEIDAMMK	EASGPINFTVFLTMFGEKLGADFEEDVITGAFKVLDPPEGKGLTIK	117	

RLC			
Human Ventricular	DYVREMLTTQAE	RFSKEEVDQMFAAFPDPVDTGNLDYKNLVHIIITHGEEND--	165
Mouse Ventricular	DYVREMLTTQAE	RFSKEEVDQMFAAFPDPVDTGNLDYKNLVHIIITHGEEND--	165
Rat Ventricular	DYVREMLTTQAE	RFSKEEVDQMFAAFPDPVDTGNLDYKNLVHIIITHGEEND--	165
Chicken Cardiac A	AYIKEMLTQEG	RFSQEEVDQMFAAFPDPVDTGNLDYKNLVHIIITHGEEND--	164
Chicken Cardiac B	DYIKEMLTQEG	RFSQEEVDQMFAAFPDPVDTGNLDYKNLVHIIITHGEEND--	163
Rabbit Skeletal	QFLEELLTTQCD	RFSQEEIKNMMAAFPDPVDTGNLDYKNLVHIIITHGEEND--	169

**Figure 9:** Amino acid sequence alignment of various isoforms of myosin regulatory light chains. Note that the residues Phe-18, Glu-22, Arg-58, and Pro-95, which are mutated in the human ventricular HCRLC of the FHC patients, are conserved across species (87). (JBC grants use without copyright permission)

Szczesna-Cordary et al. (88) have examined the physiological consequences of the E22K mutation in skinned papillary muscle fibers isolated from transgenic mice expressing human cardiac E22K-RLC mutation. They studied the FHC-associated changes in the  $\text{Ca}^{2+}$  sensitivity of cardiac muscle contraction. The first reported transgenic animal models to study FHC-associated changes in the  $\text{Ca}^{2+}$  sensitivity of cardiac muscle contraction were those expressing thin filament regulatory proteins such as tropomyosin and troponin (41, 55, 61). Szczesna-Cordary et al. (88) have shown that transgenic mice expressing the human cardiac E22K-RLC mutation experience increased  $\text{Ca}^{2+}$  sensitivity of myofibrillar ATPase activity and steady-state force development. These results are a continuation of the previous work by this group described above.

They demonstrated that the bacterially-expressed E22K mutant of the human cardiac RLC had dramatically altered  $\text{Ca}^{2+}$ -binding and phosphorylation properties compared to the WT-RLC (87). Specifically, they demonstrated that the E22K mutation, which is localized in the proximity of the RLC phosphorylation site (Ser 15) and its  $\text{Ca}^{2+}$ -binding site (residues 37-48), prevented phosphorylation of RLC and decreased its affinity for  $\text{Ca}^{2+}$  by approximately 20-fold (87). Another recent study by the same group utilizing E22K-reconstituted skinned porcine muscle preparations also showed a slight increase in the  $\text{Ca}^{2+}$  sensitivity of force and myofibrillar ATPase activity compared to WT-reconstituted preparations (88). Levine et al. (49) also studied the effect of E22K-RLC mutation on  $\text{Ca}^{2+}$  sensitivity of force in biopsied slow skeletal muscle fibers from an E22K-diseased human patient. Consistent with the work of Szczesna et al., their results showed an increase in  $\text{Ca}^{2+}$  sensitivity of force development. Since the same gene expresses the ventricular and slow-twitch skeletal muscle RLC (46), the comparison of Levine et al.'s results from study of slow skeletal fibers with the results from study of ventricular fibers by Szczesna et al. is justified (88). These current studies with E22K-animal models support the earlier work on E22K-RLC mutation, and therefore the utility of transgenic mice as an experimental system to study FHC is justified.

## 4. Rationale

### A. Reason for studying E22K-RLC mutation:

In principle, all five RLC mutations (A13T, F18L, E22K, N47K, and R58Q) can be studied. All of these mutations have demonstrated, in different experimental systems, alterations in  $\text{Ca}^{2+}$  binding, phosphorylation, and  $\text{Ca}^{2+}$  sensitivity of force and of ATPase activity (**Table 4**). The E22K-RLC mutation has been the most widely studied FHC-RLC mutation to date, having been **studied in all experimental systems** including transgenic mice (**Table 4**). Also, compared to the other mutations, the E22K-RLC mutation has shown the most **consistent and dramatic effects** on the mechanical and physiological properties of myosin in all model systems (**Table 4**). For example, the A13T and F18L mutations only cause a 2-fold decrease in  $\text{Ca}^{2+}$  binding compared to a 17-fold decline in  $\text{Ca}^{2+}$  binding in the non-phosphorylated state caused by the E22K mutation.

The E22K-RLC mutation involves the substitution of the basic lysine for the acidic glutamic acid residue. The E22K mutation occurs at the N-terminus of RLC, which is in close proximity to the C-terminal RLC-binding sequence of myosin heavy chain in the head portion of myosin. This N-terminus RLC region in the crystal structure makes a sharp bend and connects the myosin head with the myosin rod. This mutation could affect the interaction of the mutated light chain with the heavy chain of myosin. As a subunit of myosin, the RLC is known to stabilize the neck region of the myosin head, also called the lever arm. This region of the myosin head has been postulated to undergo conformational changes important for the power stroke. It is likely, therefore, that any structural



alterations in this pivotal region of myosin could affect the function of the “lever arm,” resulting in altered function of myosin cross-bridges during force generation.

An earlier study has demonstrated that the bacterially-expressed E22K mutant of human cardiac RLC had dramatically altered  $\text{Ca}^{2+}$  binding and phosphorylation properties compared with the wild-type RLC (87). Specifically, it demonstrated that the E22K-RLC could not be phosphorylated. This suggests that the phosphorylation site may be disrupted by this mutation. E22K mutation also decreased its affinity for  $\text{Ca}^{2+}$  by approximately 17 fold (87) (**Table 2 and Table 4**). It is likely that the  $\text{Ca}^{2+}$ -binding site and the phosphorylation site (Ser-15) communicate with each other, thereby affecting muscle contraction. The E22K-RLC mutation affects this intramolecular communication as  $\text{Ca}^{2+}$  is no longer able to bind strongly to its binding site. This leads to lack of phosphorylation, which in turn affects the phosphorylation-dependent effects in muscle contraction.

Another study utilizing E22K-reconstituted skinned porcine muscle preparations (90) showed a significant increase in  $\text{Ca}^{2+}$  sensitivity of force and myofibrillar ATPase activity compared to WT-reconstituted preparations (**Table 3 and Table 4**). Transgenic mice overexpressing human cardiac E22K-RLC in murine heart muscle have also demonstrated that the E22K mutation, when overexpressed in mouse cardiac muscle, increases  $\text{Ca}^{2+}$  sensitivity of myofibrillar ATPase activity and steady-state force (88).

FHC-RLC mutation	Location of the mutation	Phenotype in humans	Effect of isolated human cardiac RLC and its FHC mutants on phosphorylation and Ca <sup>2+</sup> binding	Rabbit psoas muscle fiber reconstituted with murine RLC	Porcine cardiac muscle reconstituted with human cardiac RLC	Transgenic model
A13T	Near the Ser-15 phosphorylation site in vRLC	Mid-left ventricular hypertrophy, benign, no SCD	Decreased (3-fold) Ca <sup>2+</sup> binding when RLC is non-phosphorylated. Phosphorylation increases Ca <sup>2+</sup> binding affinity	Ca <sup>2+</sup> sensitivity of force generation decreased	No effect was observed	None yet
F18L	Near the Ser-15 phosphorylation site in vRLC	Increased left-ventricular thickness, malignant, SCD	Decreased (3-fold) Ca <sup>2+</sup> binding when RLC is non-phosphorylated. No effect of phosphorylation on Ca <sup>2+</sup> binding	Ca <sup>2+</sup> sensitivity of force generation decreased. Maximal tension at saturating Ca <sup>2+</sup> concn decreased	No effect was observed	None yet
N47K	On the Ca <sup>2+</sup> binding loop	Mid-left ventricular hypertrophy, benign, no SCD reported	No binding to Ca <sup>2+</sup> when RLC is non-phosphorylated. Binding to Ca <sup>2+</sup> in phosphorylated state not determined	Not determined	Increased Ca <sup>2+</sup> sensitivity of ATPase and force, and decreased steady state force	Developed recently, did not exist at the time of our study
R58Q	Near the Ca <sup>2+</sup> binding loop	Increased left-ventricular thickness, malignant, SCD	No binding to Ca <sup>2+</sup> when RLC is non-phosphorylated. Ca <sup>2+</sup> binding was restored after phosphorylation	Not determined	Increased Ca <sup>2+</sup> sensitivity of ATPase and force, and decreased steady state force	Developed recently, did not exist at the time of our study
E22K	In between the Ser-15 phosphorylation site and the Ca <sup>2+</sup> binding loop	Mid-left ventricular hypertrophy, benign, no SCD reported	Drastic (17-fold) decrease in Ca <sup>2+</sup> binding when RLC is non-phosphorylated. E22K-RLC could not be phosphorylated	Ca <sup>2+</sup> sensitivity of force generation increased	Increased Ca <sup>2+</sup> sensitivity of ATPase, and decreased steady state force	Transgenic mice overexpressing human cardiac E22K-RLC have shown increased Ca <sup>2+</sup> sensitivity of ATPase

**Table 4:** Comparison of mechanical and physiological properties of different FHC-RLC mutations. SCD= Sudden cardiac death

One could speculate that, if binding of  $\text{Ca}^{2+}$  to the RLC plays a role in the overall  $\text{Ca}^{2+}$  homeostasis, this E22K could interfere with this process because the RLC would no longer bind  $\text{Ca}^{2+}$  with the affinity of the wild-type protein. The observed increase in  $\text{Ca}^{2+}$  sensitivity of force/ATPase in E22K fibers could be a consequence of the E22K-mediated decrease in  $\text{Ca}^{2+}$ -binding to RLC that leads to an increase in overall  $\text{Ca}^{2+}$  concentration (88). This increased  $\text{Ca}^{2+}$  levels could be utilized by troponin C, which is a key player in  $\text{Ca}^{2+}$  regulation of muscle contraction.

**B. Reasons for measuring the cross-bridge kinetics:** A recent study has shown an increase in the energy cost (ATPase/force) in a troponin mutation associated with FHC (37). This mutation is similar to the E22K-RLC mutation in that it increases  $\text{Ca}^{2+}$  sensitivity of ATPase and force. Based on this study, it is speculated the E22K-RLC mutation leads to a significant increase in the energy cost of muscle fibers from transgenic mice which express this mutation. It is generally assumed that the average force per cross-bridge does not change. In this scenario, the increase in the energy cost could be due to the change in cross-bridge kinetics. For the same amount of force generation, more ATP would be used due to increased cross-bridge cycling rates. Increased cross-bridge cycling would produce a “hypercontractile” state which would directly induce cardiac hypertrophy.

There are three primary parameters which affect the cross-bridge kinetics: 1) the rate of dissociation of force-generating myosin cross-bridges during muscle contraction ( $\tau_2$ ), 2) the rate of rebinding of the cross-bridges ( $\tau_1$ ), and 3) the rate of ADP dissociation

( $\tau_3$ ). In a cross-bridge cycle,  $\tau_2$  can be determined by measuring the rate of transition from the non force-generating state to the force-generating state. This can be achieved by measuring the rate of rebinding of cross-bridges to thin filaments. Similarly,  $\tau_1$  can be determined by measuring the rate of transition from the force-generating state back to the non force-generating state. This can be achieved by measuring the rate of dissociation of cross-bridges from thin filaments. Studies have shown that cross-bridge kinetics is altered by MLC phosphorylation, different myosin heavy-chain isoforms, load, and calcium levels (21, 55). For example, an earlier study has shown that MLC phosphorylation exerts its effect on force generation and the isometric rate of force redevelopment in striated muscle by increasing the rate of transition from non-force-generating cross-bridges to force-generating states (86).

In addition to the two mechanical parameters described above, the rate of release of ADP from the acto-myosin complex ( $\tau_3$ ) also affects the cross-bridge kinetics. This enzymatic parameter is the rate-limiting step in the actin-myosin cross-bridge cycle. Siemankowski et al. (80) estimated the release of ADP from a wide variety of sources, including different muscle types (smooth, cardiac and skeletal muscle) and different species (chicken, rat, and rabbit). Their study proposed that the rate of ADP release from myosin was a major contributor to determining the maximum shortening velocity of a muscle expressing the myosin (i.e., velocity in the absence of any mechanical load), which in turn reflects the underlying speed of the cross-bridge cycle. Previous studies have also shown differing ADP-release rates from different myosin heavy-chain isoforms



of skeletal muscle (78, 80). An earlier study with cardiac muscle has shown that the differences in V1 ( $\alpha$ -MyHC) and V3 ( $\beta$ -MyHC) cardiac myosin can be attributed to different ADP-release rates (65). A recent study by our group has proven that in contracting muscle the release of ADP is coincident with cross-bridge dissociation from thin filaments (78). Thus, if the E22K-RLC mutation increases the rate of cross-bridge kinetics, the ADP-dissociation rate would also be increased.

We have followed the mechanical and enzymatic events in the cross-bridges during force generation in the cardiac muscle of transgenic mice carrying the E22K mutation. The mechanical events have been followed by measuring the rates of rotation of the regulatory domain of cross-bridges in muscle fibers from transgenic mice containing WT or E22K-RLC. We followed the enzymatic events by measuring the rate of ADP release from the myosin active site.

### **C. Hypotheses**

In order to understand the impact of the E22K mutation in RLC on muscle contraction, we studied the kinetics of the cross-bridge cycle during force generation in the cardiac muscle of transgenic mice carrying the E22K mutation. Our research led us to propose the following hypotheses for investigation:

- 1) The E22K-RLC affects the mechanical properties of myosin by increasing the rate of cross-bridge dissociation and by increasing the rate of cross-bridge rebinding to actin during muscle contraction.

2) The E22K-RLC mutation affects the enzymatic properties of myosin by increasing the rate of ADP dissociation from the active site of myosin.

Examining the above hypotheses requires studying as few cross-bridges at a time as possible, choosing an appropriate model, establishing an experimental approach, and measuring anisotropy. These issues are discussed in detail below.

**D. Reason for studying few single cross-bridges:**

To get the most accurate information regarding cross-bridge kinetics, we would ideally like to follow the enzymatic and mechanical events in a single cross-bridge. Since techniques to study a single cross-bridge have yet to be developed, we have followed cross-bridge kinetics in a small population of cross-bridges. The characterization of motion of only a small population of cross-bridges in working muscle is important because its kinetics is not averaged over a large population of myosin heads and it avoids complications associated with molecular crowding which may influence the structure and function of the myosin molecule studied in isolation.

Expression levels of mutated proteins in transgenic mice carrying FHC-causing mutation differ. Human patients are heterozygous for FHC mutations, so their thick filaments are composed of WT myosin heads interspersed with mutant heads. Any large observational volume contains a mixture of fast (WT) and slow (FHC) molecules, making the comparison between the kinetics of healthy and diseased muscle impossible. **Figure 10** explains the concept in more detail.

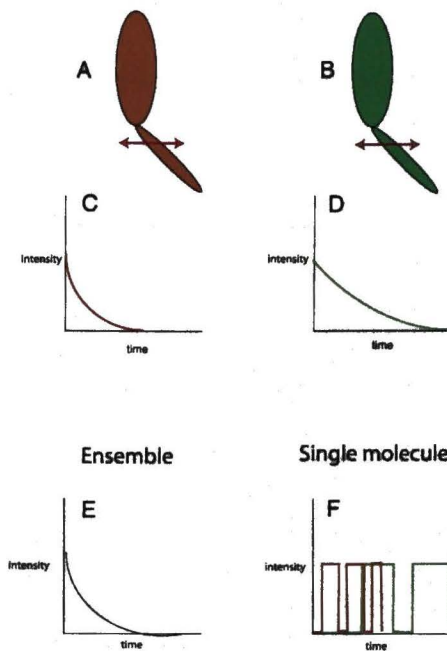


**Figure 10.** Importance of measuring single-head kinetics. Suppose WT heads are fast (**A**, red) and mutated heads are slow (**B**, green). The relaxation of fast heads, as measured by the orientation of the transition dipole (arrow), is fast (**C**) and the relaxation of slow heads is slow (**D**). The rate of relaxation of a large ensemble of heads will be a weighted average of slow and fast relaxations (**E**). It is impossible to tell from such a curve whether relaxations of mutated and non-mutated heads are different. If, on the other hand, kinetics of a single molecule is measured, there will be little difficulty in distinguishing the kinetics (**F**). (Courtesy J. Borejdo)

Measuring the orientation of a single cross-bridge among the trillions present in even a short segment of isolated cardiac muscle fiber is a complex endeavor. Data must be collected from a volume of muscle small enough to contain few cross-bridges. An important development in this process was the introduction of small observational volumes defined by diffraction-limited laser beams and confocal detection which made it possible to limit the observational volume to a femtoliter ( $10^{-15}$  L) and eliminate much of the background noise.

**Figure 11** shows the detection volume of confocal microscope. It is approximately 0.3 micron wide (defined by diffraction limit) and approximately 0.3 micron thick (defined by confocal aperture). Such volume contains on average approximately 400 cross-bridges. By using sudden release of ATP from a caged precursor, cross-bridges become synchronized so that they behave like one cross-bridge. Spectroscopic methods offer a convenient way to measure mechanical (95) and enzymatic (18, 79) events. In particular, fluorescence polarization or anisotropy (1, 8, 11, 16, 19, 24, 25, 35, 36, 41, 63, 73, 92) provides information about binding and orientation of the myosin head and of the lever arm.

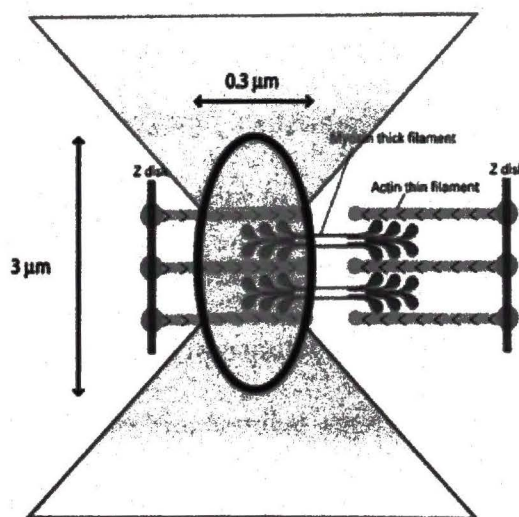


**Figure 11:** Schematic of the illumination volume impinging on the muscle (adapted courtesy of J. Borejdo)



#### **E. Reason for choosing transgenic mice for the experimental model:**

The overall goal of this study was to understand the effect of FHC-RLC mutations on muscle contraction by studying the kinetics of the cross-bridge cycle during force generation. Cardiac muscle fibers expressing FHC-causing RLC mutations were needed for our research. At the time of this study, the E22K-RLC mutation was the only RLC mutation which had been expressed in transgenic mice. The human phenotype was also recapitulated by these transgenic E22K-mutant mice, although an echocardiographic examination and heart weight to body weight ratios did not produce any differences. Thus, transgenic mice expressing the E22K-RLC mutation helped in understanding the influence of FHC-producing RLC mutations on cross-bridge kinetics. This in turn helped in understanding the physiological role of RLC in the regulation of cardiac muscle contraction.

#### **F. Reason for studying skeletal muscle:**

The study's experimental approach was established by performing experiments on skeletal muscle prior to beginning experiments on cardiac fibers. In contrast to cardiac fibers, skeletal fibers are much easier to work with because their simpler organization of fibers arranged in parallel arrays makes them easier to observe. They are also more amenable to biochemical manipulation, such as that produced by attaching a fluorescent probe. Previous work from our lab has demonstrated the replacement of endogenous ELC as well as endogenous RLC with fluorescently-labeled ELC and RLC (10, 77). In these

studies approximately 1-2% of cross-bridges were fluorescently labeled. These studies with fluorescently-labeled ELC or RLC have demonstrated changes in anisotropy which leads us to believe that cross-bridges carrying these labeled ELC are active.

**G. Reason why anisotropy was measured:**

Fluorescence polarization or anisotropy provides information about binding and orientation of the myosin head and of the lever arm. A fluorescent dye is attached to a specific molecule, such as RLC, and anisotropy follows and records via the dye the movement of RLC. By nature, fluorescent dyes exhibit a dipole moment or direction. It is the direction or orientation of the dye on the RLC which is measured. Anisotropy ( $I$ ) is a ratio of the horizontal ( $I_{\parallel}$ ) and vertical ( $I_{\perp}$ ) emission intensities of the dye, where  $I = (I_{\parallel} - I_{\perp}) / (I_{\parallel} + 2I_{\perp})$ . Anisotropy is plotted as graph of anisotropy in arbitrary units (a.u.) over time.

For this study the anisotropy technique was exploited to examine the effect of the E22K mutation in RLC on kinetics of cross-bridges in Tg-E22K mouse fibers compared to non-Tg and Tg-WT fibers. Depending on the position of the fluorescent probe on myosin or actin, its anisotropy indicates dissociation of myosin heads from thin filaments, cross-bridge re-binding to actin, or an enzymatic event occurring on the myosin active site. The cross-bridge dissociation was determined from the increase in the rate of rotation of actin monomer to which a cross-bridge was bound. With dissociation, the actin monomer begins to rotate because its rotation is no longer restrained by myosin (10, 12). Re-binding was measured from the rate of anisotropy change of the rhodamine-

labeled recombinant essential light chain of myosin (Rh-LC1) exchanged for the native LC1 in cardiac myofibrils. Thus, the lever arm of myosin contained both hypertrophy-causing mutated RLC and fluorescent LC1.

The rate of ADP dissociation from the active site of myosin was determined from anisotropy of muscle pre-loaded with a stoichiometric amount of fluorescent ADP. ADP starts rotating rapidly once it is liberated from the immobile myosin by sudden release of excess non-fluorescent ATP. The rate of release can be monitored by measuring anisotropy of fluorescence because free ADP rotates faster than ADP immobilized by myosin (77).

## CHAPTER II

### MATERIAL AND METHODS

#### 1. Methods for Studying Skeletal Muscle

**Chemicals and solutions:** Standard chemicals were obtained from Sigma (St Louis, MO). Five-dimethoxy-2-nitrobenzyl-caged ATP (DMNPE-caged ATP), 5'-iodoacetamido-fluorescein (IAF), and 5'-iodoacetamido-tetramethylrhodamine (IATR) were obtained from Molecular Probes (Eugene, Oregon). The glycerinating solution contained 80 mM K-Acetate, 0.2 mg/mL phenylmethylsulfonyl fluoride (PMSF), 2 mM  $\beta$ -mercaptoethanol, 4 mM  $\text{MgCl}_2$ , 5 mM ATP, 2 mM ethylene glycol-bis( $\beta$ -aminoethyl) ether (EGTA), 1 mM dithiothreitol (DTT), and 10 mM Tris-HCl at pH = 7.6 in 50% glycerol. The rigor solution contained 50 mM KCl, 4 mM  $\text{MgCl}_2$ , 0.1 mM  $\text{CaCl}_2$ , 1 mM DTT, and 10 mM T-HCl at pH = 7.6. The relaxing solution contained 50 mM KCl, 4 mM  $\text{MgCl}_2$ , 2 mM ATP, 2 mM EGTA, 1 mM DTT, and 10 mM Tris-HCl at pH = 7.6. All the solutions used in the photolysis experiments contain 10 mM reduced glutathione.

**Psoas muscle isolation from rabbits:** The psoas muscle was isolated from isoflurane-anesthetized young adult New Zealand White rabbits and stored in glycerinating solution at  $-20^\circ\text{C}$  for no more than 3-5 months.



**Expression and purification of LC1 (ELC):** *E. coli* M15[pREP4] cells (Qiagen) were used for expression of the LC1, which was cloned with pQE60 vector using a DNA polymerase chain reaction with the 3'-end containing a tag of 6 histidines. Cloning of LC1 has been done previously (14). Glycerol stocks of M15 *E. coli* cells containing the pQE60 vector with LC1 insert were used to streak on agar plates containing 100 µg/mL of ampicillin and 25 µg/mL of kanamycin. After growing overnight at 37°C, single-cell colonies were transferred into 20 mL LB media containing antibiotics. To express LC1, 20 ml of overnight cell culture were transferred to 1 L of LB media containing 100 µg/ml of ampicillin and 25 µg/mL of kanamycin grown to  $OD_{450} = 0.5$ . Then the expression was induced by addition of 1 mM of isopropyl-β-D-thiogalactoside (IPTG). After 4 hours of expression, the cells were collected by centrifugation at 4,000xg for 20 minutes, frozen in liquid nitrogen, and stored at -20°C until purification.

Batch purification under denaturing conditions recommended by Qiagen was used to isolate expressed LC1. The expressed LC1 was purified on the Ni-NTA (Nickel-nitrilotriacetic acid) columns under denaturing conditions. The frozen cell pellet was incubated on ice for 15 minutes and then resuspended in buffer B (Lysis Buffer-8 M urea, 10 mM Tris-Cl, and 100 mM  $NaH_2PO_4$  at pH = 8.0) at 5 mL per gram wet weight. The cells were stirred for 60 minutes and then centrifuged at 10,000xg for 20 minutes. 1 mL of 50% Ni-NTA agarose slurry (Qiagen) was added to 4 mL of cleared lysate and mixed by gently shaking for 60 minutes. The lysate-resin mixture was loaded into empty columns and the flow-through was collected. The column was washed with two volumes of buffer C (the wash buffer is the same as buffer B but with a pH = 6.3). The LC1 was

eluted with one volume of buffer D (the elution buffer is the same as buffer B but with a pH = 5.9) and then with one volume of buffer E (the elution buffer is the same as buffer B but with a pH = 4.5). The purified LC1 was analyzed by SDS-PAGE (sodium dodecyl sulfate-polyacrylamide gel electrophoresis) and used for labeling or freeze dried in the presence of an equal weight of sucrose and stored at -20°C.

**Labeling of LC1 and exchange into fibers:** The LC1-containing solution was dialyzed against buffer A (50 mM KCl and 10 mM phosphate buffer at pH = 7.0). LC1 were labeled by incubation with 5-times molar excess of 5'-IATR for 6 hours in buffer A at 4°C. The stock solution of IATR dissolved in methanol was prepared just before the experiment was initiated. Excess IATR was removed by passage over Sephadex G50 column, followed by dialysis against standard buffer (50 mM KCl and 10 mM Tris at pH = 7.6). Analysis showed that 3.5-7% of purified protein was fluorescently labeled.

Rh-LC1 was exchanged into fibers by incubating 1 mg/mL Rh-LC1 in light-chain exchange solution (150 mM KCl, 5 mM ethylene-diamine-tetra-acetic acid (EDTA), 5 mM DTT, 10 mM  $\text{KH}_2\text{PO}_4$ , 5 mM ATP, 1 mM tri-fluoroperazine (TFP), and 10 mM imidazole at pH = 6.5) with 1 mg/mL in the same solution for 0.5 hours at 30°C (84). The degree of labeling was estimated by comparing the intensity of fluorescence of fibers that underwent exchange with the intensity of a known concentration of labeled light chains. The concentration of dye in muscle was  $\sim 3 \mu\text{M}$  (i.e., 2.5% of cross-bridges contained fluorescent Rh-LC1).

**Labeling of the myosin active site:** The myosin active site was labeled with 1  $\mu\text{M}$  Alexa-ATP in  $\text{Ca}^{2+}$  rigor for 10 minutes at room temperature. The excess dye was extensively washed out with rigor solution.

**Labeling of F-actin:** Actin filaments were labeled with rhodamine-phalloidin (Rh-Ph) by incubating the fibers in rigor solution with 1  $\mu\text{M}$  of Rh-Ph for 10 minutes at room temperature. After labeling, the fibers were extensively washed with the  $\text{Ca}^{2+}$  rigor solution.

**Preparation and mounting of skeletal muscle fibers:** Isolated muscle fibers were prepared from glycerinated rabbit psoas muscle bundles by dissecting single fibers in glycerinating solution and attaching the ends of the tautly-stretched fiber to aluminum clips glued to a microscope coverslip. This was followed by labeling either the actin or the LC1. A glass cover slip was placed over the fiber and rested on  $\sim 2$  mm layer of Vaseline lined along the edge of the microscopic slide to prevent evaporation and drying of the fiber.

**Force tension measurements:** This measurement was performed to ensure that the fibers were viable and that the transgenic fibers developed the same force as normal fibers. A MKB force transducer (Scientific Instruments, Heidelberg, Germany) was coupled to an analog counter (Model 6024E, National Instruments, Austin, TX). Isometric contraction was recorded in fiber strips stretched to approximately 1.2 times slack length after mounting between a fixed arm and a force transducer.

**Anisotropy measurements:** Anisotropy of myosin and actin after release of ATP from the cage was recorded. Anisotropy change was divided into two phases. The half-times of

the first phase, indicating cross-bridge dissociation, and that of the second phase, corresponding to a slow relaxation back to a rigor, were measured in milliseconds using SigmaPlot 7.101. The point at which pulse was administered (denoted by a deflection in polarized-emission intensities or anisotropy) until the inflection stopped denoted the first phase. The point at which the inflection returned towards the original value until approximately 3-4 seconds later denoted the second phase. Anisotropy was detrended to account for photobleaching effects and also examined on an expanded scale (a one-second as compared to a seven-second time scale) to inspect the trend more closely.

**Confocal microscopy:** The confocal laser scanning microscope LSM 410 (Carl Zeiss) mounted with water immersion Zeiss Planochromat Korr W 40X objective was used to study the localization of light chains exchanged into muscle fibers. 5'-IATR and 5'-IAF were excited with argon laser at 568 nm and 488 nm, and emissions were registered at 590 nm and 515 nm respectively.

**Photogeneration of ATP:** Muscle was perfused with 2 mM of DMNPE-caged ATP. The UV beam was focused by the objective to a Gaussian spot with width and length equal to twice the lateral resolution of the UV beam (about 0.2  $\mu\text{m}$ ). The height of focus of the objective was  $\sim 3 \mu\text{m}$ . A few seconds after initiating the experiment, the shutter admitting the UV light was opened for exactly 10 msec and 0.12 mJ/sec was incident on the muscle. Because of the clipping of the enlarged laser beam by the entrance aperture of the objective, loss at the mirror (Dichroic Mirror1) and loss due to absorption by glass in the objective occurred. The area illuminated by UV was  $0.04 \mu\text{m}^2$ . The energy flux at the illuminated area was  $0.12 \text{ mJ} / (\text{sec} \times 0.04 \mu\text{m}^2) = 3.0 \text{ mJ} / (\text{sec} \times \mu\text{m}^2)$ . ATP stayed in the



experimental volume for 300  $\mu\text{sec}$  on average. The energy through the illuminated area at this time was  $9 \times 10^{-4} \text{ mJ}/\mu\text{m}^2$ , greater than the energy flux obtainable with a frequency-doubled ruby laser (approximately  $3 \times 10^{-5} \text{ mJ}/\mu\text{m}^2$ ) (35). The high energy flux of the UV laser allowed illumination of a smaller cross-sectional area of the fiber, which in turn helped limit the number of cross-bridges studied.

**The amount of photoreleased ATP:** The amount of ATP produced in a single experiment was estimated by measuring the luminescence of luciferin-luciferase solution exposed to a UV beam. A 10  $\mu\text{L}$  sample of rigor solution containing 2 mM caged ATP was illuminated by a 0.12 mW UV beam for 1, 30, and 60 seconds. Then 5  $\mu\text{L}$  of 40 mg/mL LL was placed on an X-ray film (Kodak) and mixed with 5  $\mu\text{L}$  of solution containing photogenerated ATP. The film was exposed for 10 minutes. The calibration curve was obtained by mixing known amounts of ATP with luciferin-luciferase solution. The film was scanned by a MicroTek scanner and the optical density measured by Image Plus Pro (Media Cybernetics, Silver Spring, MD). During the one-second exposure,  $10^{-12}$  moles of ATP were produced. Therefore, allowing for UV absorption by the glass cover slide, at least  $10^{-15}$  moles were produced in  $0.3 \mu\text{m}^3$  within 10 msec, enough to convert all the precursors to ATP.

**Heat generation:** The most significant source of possible artifacts is heating, which is caused by the absorption of UV light by caged ATP. The extinction coefficient of caged-ATP at 364 nm is  $4,400 \text{ M}^{-1}\text{cm}^{-1}$ , (i.e., a 3- $\mu\text{m}$  thick section of muscle perfused with 2 mM precursor absorbs  $1 - \exp[-3 \times 10^{-4} \times 4.4 \times 10^3 \times 2 \times 10^{-3}] = 0.00264$  of the UV light). However, the heat associated with this absorption dissipates rapidly ( $\sim 70 \text{ nsec}$ )

from the experimental volume because the beam diameter is small (23). The UV laser delivers 0.12 mJ/sec (i.e.,  $0.9 \times 10^{-11}$  J in 70 nsec). The experimental volume weighs  $\sim 10^{-12}$  g. Because  $4.2 \times 10^{-12}$  J are required to heat  $\sim 10^{-12}$  g by  $1^{\circ}\text{C}$ , the temperature rise during an experiment is less than  $2^{\circ}\text{C}$ . Three additional lines of evidence suggested that the anisotropy change did not reflect temperature rise in the experimental volume: 1) there was no anisotropy change in skeletal muscle due to caged EDTA, 2) there was no anisotropy change in denatured skeletal muscle fibers, and 3) there was no anisotropy change in skeletal fibers devoid of myosin upon stimulation by caged ATP (not shown).

## 2. Methods for Studying Cardiac Muscle

**Mice:** Transgenic mice expressing human cardiac Wt-RLC and E22K-RLC were given as a gift by Dr. Danuta Szczesna (University of Miami). These mice showed 30-90% transgenic protein expression.

**Preparation of myofibrils:** Myofibrils were prepared according to the modified method of Solaro (82). The final storage conditions were 50% glycerol: 50% standard myofibril buffer (30 mM imidazole, 60 mM KCl, and 2 mM  $\text{MgCl}_2$  at pH = 7.0).

**Exchange of LC1 into myofibrils:** Rh-LC1 was exchanged into myofibrils by incubating 1 mg/mL Rh-LC1 in light-chain exchange solution (150 mM KCl, 5 mM EDTA, 5 mM DTT, 10 mM  $\text{KH}_2\text{PO}_4$ , 5 mM ATP, 1 mM TFP, and 10 mM imidazole at pH = 6.5) with 1 mg/mL myofibrils in the same solution for 0.5 hours at  $30^{\circ}\text{C}$  (83). The degree of labeling was estimated by comparing the intensity of the fluorescence of the fibers that underwent exchange with the intensity of a known concentration of labeled

light chains. The concentration of dye in myofibrils was  $\sim 3 \mu\text{M}$  (i.e., 2.5% of cross-bridges contained fluorescent Rh-LC1).

**Labeling of the myosin active site:** The myosin active site was labeled with  $1 \mu\text{M}$  Alexa-ATP in  $\text{Ca}^{2+}$  rigor for 10 minutes at room temperature. The excess dye was extensively washed out with rigor solution.

**Labeling of F-actin:** Actin filaments were labeled with rhodamine-phalloidin (Rh-Ph) or fluorescein-isothiocyanate (FITC)-phalloidin by incubating the fibers in rigor solution with  $1 \mu\text{M}$  of Rh-Ph for 10 minutes at room temperature. After labeling, the fibers were extensively washed with the  $\text{Ca}^{2+}$  rigor solution.

**Measuring anisotropy of cardiac myofibrils:** Fluorescence was measured with a high aperture lens (C-Apo, 40X magnification, Numerical Aperture = 1.2). Calculations showed that high numerical aperture of the objective results in minimal distortion to the polarized intensities. The subscripts after the intensity ( $\perp I_{\perp}$  &  $\perp I_{\parallel}$ ) indicated the direction of the polarization of the emitted light relative to the axis of the muscle fiber. The subscript before intensity indicated the direction of the excitation light. This direction was always perpendicular to the axis of myofibril. Then the photomultipliers 1 and 2 were recorded as  $\perp I_{\perp}$  and  $\perp I_{\parallel}$  respectively. The microscope was operated in a “spot” mode (i.e., a single spot, located exactly in the center of the field of view, was illuminated). The beam was not scanned. To minimize photobleaching, the laser light was attenuated 100 times (the power incident on the fiber =  $23 \mu\text{W}$ ). The details of the experimental arrangement are given below (10). Only the myofibrils which were aligned horizontally on the stage were chosen for experiments. Polarization varied as  $\cos^2 A$ , where A is the



angle that the myofibrillar axis made with the horizontal axis. Since the myofibrils were lying horizontally, the angle that the myofibrillar axis made with the horizontal axis was small, thus producing very low variation.

**Muscle protein purification:** Porcine muscle myosin was isolated as described above (96). Rabbit skeletal muscle actin was isolated using the method described by Pardee and Spudich (64). For actin purification, rabbit psoas muscle was minced followed by extraction with KCl, NaHCO<sub>3</sub>, EDTA, H<sub>2</sub>O, and acetone. The acetone extract was dried to produce acetone powder from which actin was purified through extraction, filtration, centrifugation, and polymerization. During extraction, 1 g of acetone powder was extracted with 20 mL of Buffer A (2 mM Tris-HCl, 0.2 mM ATP, 1 mM DTT, and 0.2 mM CaCl<sub>2</sub>) for 30 minutes by stirring on ice. The extract was then filtered and residue washed with 10 mL of Buffer A. This extract was again filtered and the two extracts were mixed before centrifugation at 36,000xg (~20k rpm) for one hour at 4°C. The supernatant was polymerized for 2 hours at 4°C, followed by high salt (50 mM KCl and 2 mM MgCl<sub>2</sub>) incubation for 30 minutes at 4°C. This was followed by further centrifugation at 70,000xg for 3 hours at 4°C. The pellet was then dialyzed with Buffer A for 48 hours at 4°C followed by further centrifugation at 80,000xg for 3 hours at 4°C. This process yielded supernatant containing G-actin which was allowed to polymerize for 2 hours at 4°C without stirring.

**Anisotropy of solutions:** LC1 of isolated myosin, prepared according to Tonomura et al. (96), was exchanged with Rh-LC1 (50). Fluorescence anisotropy was measured in a K2 spectrofluorometer (ISS, Champaign, Illinois). To avoid scattered light, a 500 nm cut-off



filter was used in the emission channel. All measurements were performed using magic-angle conditions at 0°C. All the samples used in the fluorescence measurements had absorption of  $< 0.1$ .

**Lifetime measurements:** These measurements were performed with Fluo Time 200 Fluorescence Lifetime System (PicoQuant, Berlin, Germany) together with a picosecond laser system. Actin was labeled with fluorescein-phalloidin at 1:1 molar ratio.

**Statistical Analysis:** Means and standard deviations were determined from the anisotropy data. To determine significance, the data obtained were submitted to the one-way analysis of variance test (ANOVA) and the Tukey-Kramer multiple comparison test using the GraphPad Instat<sup>®</sup> software (version 3.01). Results were considered statistically significant at  $P \leq 0.05$ .

## CHAPTER III

### DEVELOPMENT OF EXPERIMENTAL APPROACH USING SKELETAL MUSCLE

This chapter presents the results of the experiments performed on skeletal muscle to establish our experimental approach. The skeletal fibers have a simple architecture and are easily amenable to biochemical manipulations such as labeling with a fluorescent probe. The orientation changes of the regulatory domain during power stroke in skeletal muscle were measured. More specifically, the rate of the dissociation of myosin heads from actin ( $1/\tau_1$ ) and the rate of cross-bridge rebinding ( $1/\tau_2$ ) was measured by studying a small population of cross-bridges in skeletal muscle. Cross-bridge dissociation was synchronized by rapid application of ATP, and the orientation changes associated with binding and hydrolysis of a single molecule of ATP were followed through anisotropy measurements. The muscle was labeled with fluorescent phalloidin to measure  $\tau_1$ . The muscle was labeled at the regulatory domain by replacing native ELC with fluorescently-labeled recombinant ELC to measure  $\tau_2$ .

**Labeling of myosin and actin in skeletal myofibrils.** Figure 1 shows a confocal image of fluorescently-labeled skeletal fibers. Actin in skeletal fibers was labeled with FITC-phalloidin. Myosin in skeletal fibers was exchanged with Rh-LC1 and Rh-phalloidin as described in the Methods section. The degree of labeling was ~3-5% for Rh-LC1. The microscope had no trouble detecting such lightly labeled fibers. Labeled ELC was exchanged with endogenous light chains into fibers and experiments were performed to

verify that labeled light chains were indeed exchanged into fibers while the endogenous protein was extracted. This procedure is based on the fact that molecules can reversibly dissociate from their binding sites and be replaced by externally applied proteins competing for the free-binding sites. Furthermore, the labeled exogenous protein specifically folds into the site due to its conformational affinity for the binding site.

**Figure 2** demonstrates that the exchange successfully introduces fluorescent LC1 into muscle without extracting other proteins. Lanes 1-4 show the SDS gel of skeletal muscle exchanged with fluorescent light chains stained with Sypro Ruby protein stain. Lane 2 is a skeletal muscle fiber showing myosin (Myo), actin (Act) and light chains (LC 1-3). After incubation for 0.5 hours at 30°C in extraction solution (lane 3), the lanes 2 and 3 of the Sypro stained gel are identical. Previous studies have shown that TFP promotes depletion of native LC1 only when the LC1 is also included in the buffer exogenously (84). Thus, when the fiber is incubated in extraction buffer (which lacks exogenous LC1), LC1s are not dissociated from the heavy chain. When muscle is incubated for 0.5 hours at 30°C in exchange solution (lane 4; identical to extracting solution but containing 1 mg/mL recombinant fluorescent LC1), the Sypro staining shows no difference once again (compare lanes 3-4). However, when viewed under fluorescent light, the fluorescent LC1 is observed in the skeletal exchanged lane (lane 8). LC1 incorporates more efficiently into skeletal than into cardiac muscle. Western blots using anti-LC1 antibody (lanes 9-11) identify fluorescent bands as LC1. This result proves that the exchange successfully introduces fluorescent LC1 into muscle. Incidentally, control experiments (not shown) reveal that if the extracting solution contained no TFP, no exchange occurred.

The procedure for ELC exchange in permeabilized rabbit muscle fibers was based upon functional studies that have showed normal function of fibers upon endogenous ELC removal and re-addition of recombinant ELC (84). The structural effects of the light-chain removal and recombinant exchange into myosin were not examined beyond force-tension experiments, myofibril exchange, and visual striation patterns using confocal microscopy. The effect of ELC exchange on the X-ray pattern from contracting fibers is unknown.

**Functionality of exchanged fibers:** This measurement was performed to ensure that the fibers were viable and that the transgenic fibers developed the same force as normal fibers. Control (unlabeled) fibers developed normal maximum isometric tension ( $0.94 \pm 0.05$  mN/fiber, mean  $\pm$  SD with  $n = 32$ ). Fibers exchanged with fluorescently labeled LC1 developed 90% of the isometric tension developed by control fibers ( $0.81 \pm 0.04$  mN/fiber). The lack of effect on tension is consistent with previous experiments with such fibers and with experiments that used chicken gizzard RLC labeled at Cys 108 (1, 50, 73).

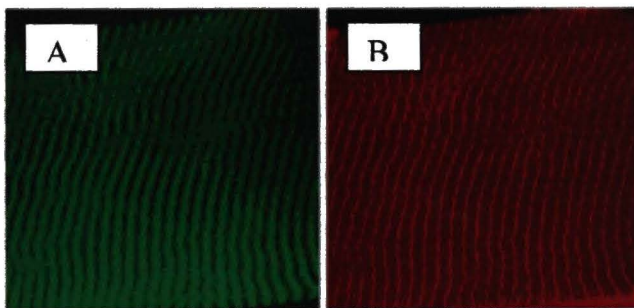


**Figure 1:** Confocal image of fluorescently labeled skeletal fibers: Actin labeled with FITC-phalloidin (green, A) and myosin labeled with essential light chain coupled to IATR (red, B) in the same muscle fiber.



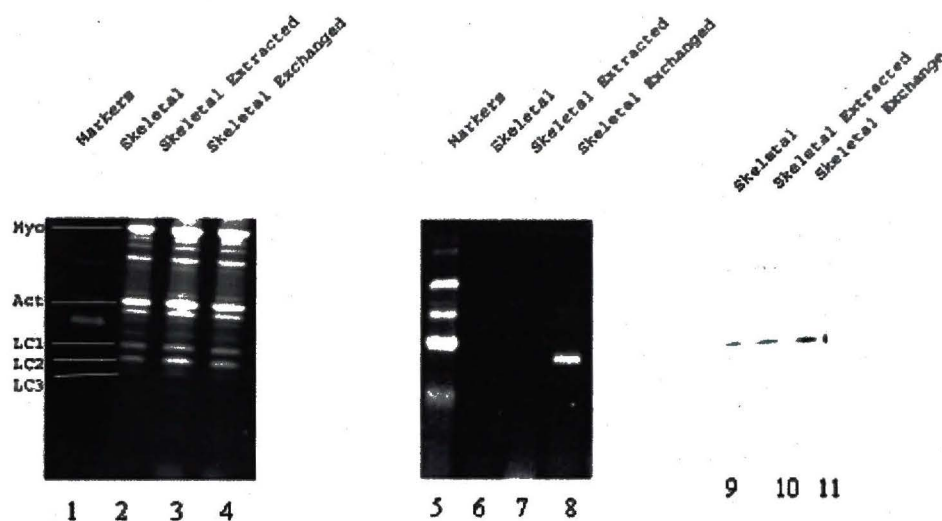


**Figure 2:** Incorporation of fluorescent light chains into skeletal muscle.

Lanes 1-4: SDS gel stained with Sypro Ruby Protein Stain.

Lane 1: Protein markers 20KD, lane 2: rabbit psoas muscle fiber, lane 3: muscle fiber after incubation in extracting solution for 0.5 hrs, lane 4: muscle fiber after incubation in exchanging solution for 0.5 hrs containing recombinant fluorescent LC1.

Lanes 5-8: SDS gel stained viewed under fluorescent light before staining with Sypro Ruby Protein Stain. Lanes correspond to lanes 1-4.

Lanes 9-11: Western blots stained with anti-LC1 antibody. The samples are identified above each lane.

### **Changes of anisotropy of actin labeled with Rh-phalloidin:**

The experimental approach was to observe a small population of actin monomers, to synchronize motion by rapid application of ATP, and to follow the orientation changes associated with binding and hydrolysis by myosin of a single molecule of ATP. Muscle actin was labeled with Rh-phalloidin and the fiber was placed horizontally on a stage of a confocal microscope.

The rotations were synchronized by the sudden photogeneration of ATP from a caged precursor. Approximately three seconds after initiating the experiment, the shutter admitting the UV light was opened for exactly 10 msec, producing 2 mM ATP in the illuminated volume. The diffusion coefficient of ATP is  $3.7 \times 10^{-6} \text{ cm}^2 \text{ per second}$  (40), so ATP diffused away from the experimental volume in  $\sim 300 \text{ } \mu\text{sec}$ . Although the actual diffusion coefficient in filament lattice of muscle fiber may be smaller, the order of the magnitude of the calculation shows that soon after the application of pulse, there is practically no free nucleotide in the experimental volume. The sole nucleotide remaining in the volume is bound to the cross-bridge. The anisotropy change after the release of ATP from its caged precursor reflects cross-bridge dissociation from actin.

**Figure 3A** shows a typical record of perpendicular anisotropy change. Upon rapid (10 msec) release of ATP from the cage (**Figure 3A**, arrow) anisotropy drops rapidly, indicating dissociation of cross-bridges from thin filaments. The time was measured by drawing the dissociation curve on an expanded time-scale (**Figure 3B**) and estimating the

time it took for anisotropy to decay from the maximum to the minimum. In eight experiments, the time of dissociation of cross-bridges from actin was  $140 \pm 20$  (mean  $\pm$  SD) msec. This result is consistent with the earlier work in skeletal muscle from our lab (10, 12).

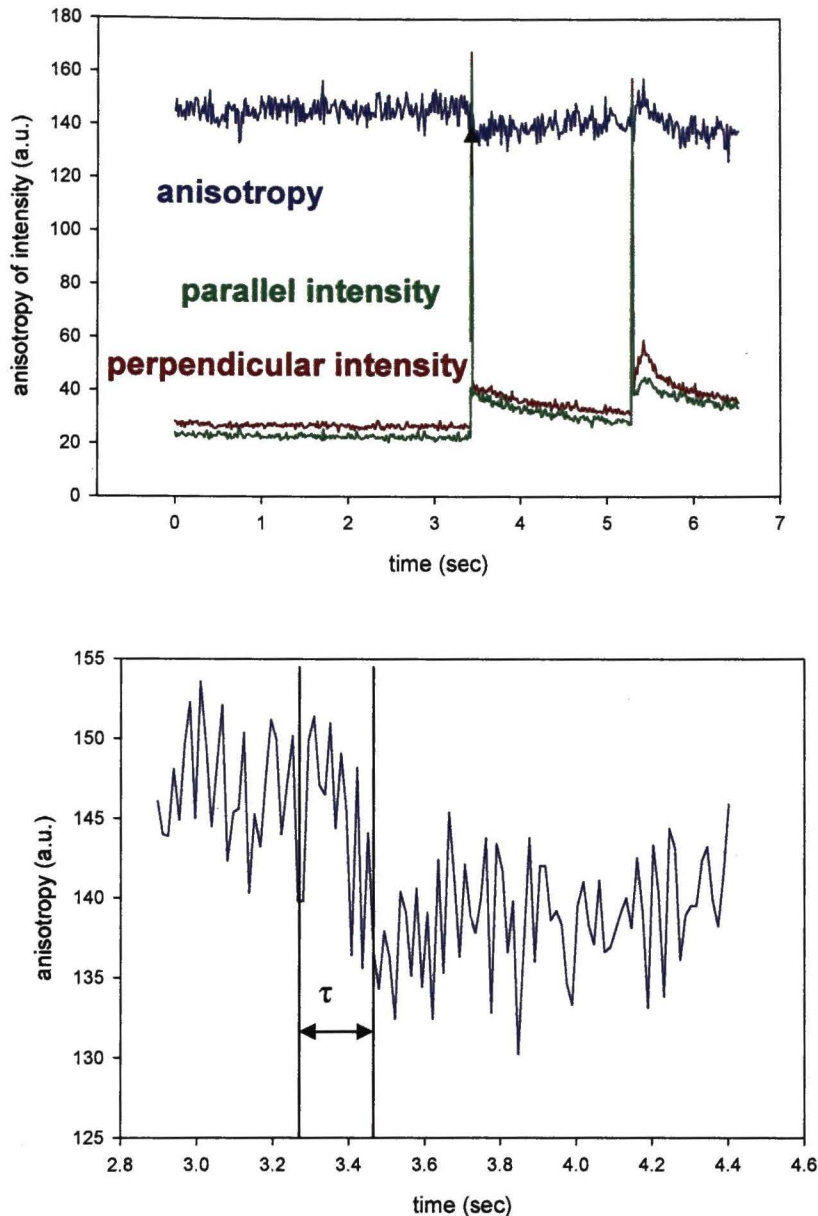


**Figure 3.** Time course of change of perpendicular anisotropy of muscle labeled with Rh-Ph. Muscle is initially in rigor. Sudden pulse applied at arrow generates ATP and causes single turnover of cross-bridges. **A)** Orthogonal intensities (red and green) and anisotropy (blue). “Parallel” and “perpendicular” refers to the orientation of polarization of linearly-polarized fluorescent (emitted) light relative to the long axis of a myofibril. **B)** The drop of anisotropy indicates cross-bridge dissociation from thin filaments. The vertical lines were fitted by inspection. The distance between them is equal to the dissociation time.



### **Changes of Anisotropy of Essential Light Chain Labeled with IATR:**

The time course of orientation changes of cross-bridges was measured by anisotropy of recombinant fluorescent LC exchanged with native ELC in a muscle fiber. Following dissociation, cross-bridges rebind to thin filaments, as indicated by the slow exponential rise of anisotropy (**Figure 4A**). To correct for photobleaching, the initial decline of the anisotropy curve (between points a and b) was fitted to an exponential. This exponential fit was subtracted from the original data, giving a corrected rise of anisotropy. A typical corrected curve is shown in Figure 4B. This corrected anisotropy was fitted by a three-parameter exponential curve,  $y = y_0 + ae^{-bx}$ . This procedure was applied to all muscles labeled with Rh-LC1. The rate of rotation of the myosin lever arm,  $1/\tau_2$  was  $0.48 \pm 0.18$  (mean  $\pm$  SD)  $\text{sec}^{-1}$ . This is consistent with the previous work from our lab in which showed similar rate of rotation of the myosin lever arm (14).

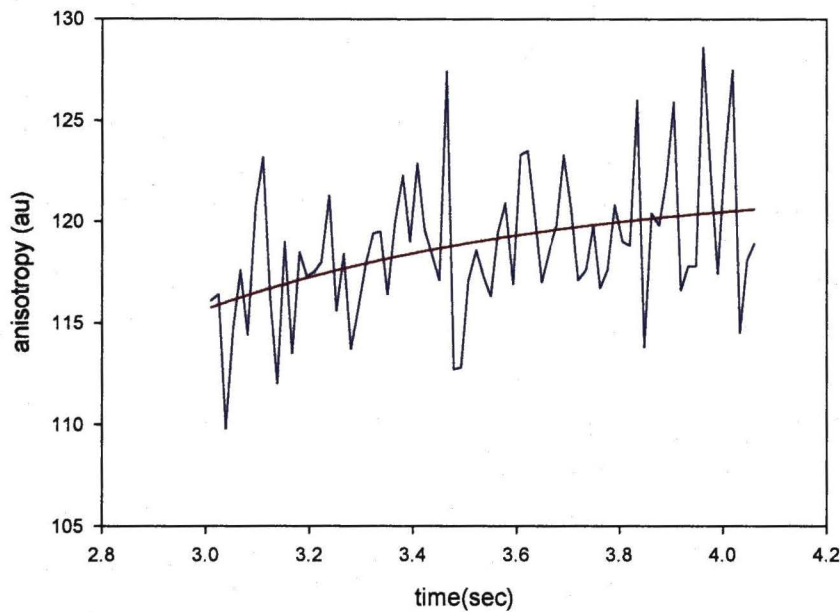
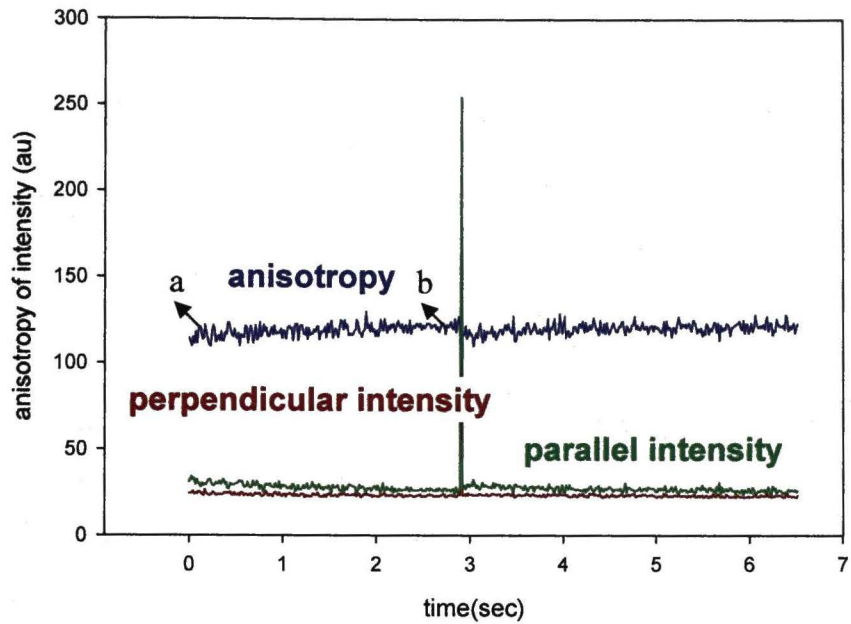


**Figure 4.** Time course of change of perpendicular anisotropy of muscle labeled with Rh-LC1. During the time interval from a to b, muscle is in rigor. Sudden pulse of UV light is applied at point b to create ATP and cause cross-bridges to undergo one turnover cycle. **A)** Orthogonal intensities and anisotropy. **B)** The rise of anisotropy, indicates cross-bridge re-binding to thin filaments. To account for photobleaching, the anisotropy between points a and b was fitted to a curve and the data subtracted from it. As a result, the “de-trended” data begins at 0. The data was fitted to an exponential rise to a maximum  $y = 107.8 + 13.9(1 - e^{-0.65t})$ .

## CHAPTER IV

### EFFECT OF E22K-RLC MUTATION ON CARDIAC MUSCLE FUNCTION

#### 1. Cardiac Myofibril Measurements

In this experiment we used transgenic mouse cardiac myofibrils expressing the human isoform of  $\nu$ RLC to study the influence of E22K-RLC mutation. The following parameters were studied: (i) dissociation time,  $\tau_1$ , of myosin heads from thin filaments, (ii) re-binding time,  $\tau_2$ , of the cross-bridges to actin, and (iii) dissociation time,  $\tau_3$ , of ADP from the active site of myosin. Time  $\tau_1$  was determined from the increase in the rate of rotation of actin monomer to which a cross-bridge was bound. Time  $\tau_2$  was determined from the rate of anisotropy change of the recombinant essential light chain of myosin labeled with rhodamine (Rh-LC1) exchanged for native LC1 in the cardiac myofibrils. Time  $\tau_3$  was determined from anisotropy of muscle pre-loaded with a stoichiometric amount of fluorescent ADP, which starts rotating rapidly once ADP is released from immobile myosin by sudden release of excess non-fluorescent ATP. The cross-bridges were activated by a precise delivery of ATP from a caged precursor. The rates were measured in transgenic-mutated (Tg-m) heart myofibrils overexpressing the E22K mutation of human cardiac RLC in transgenic wild-type (Tg-wt) and non-transgenic (non-Tg) muscles.

We also measured binding affinity of fluorescently-labeled actin with Tg-wt and

Tg-m myosin by measuring changes in lifetimes when purified fluorescently-labeled actin is bound to myosin carrying wt-RLC or E22K-RLC. A lifetime is a sensitive measure of conformation because it is very sensitive to environmental changes. If the mutation altered the binding characteristics of myosin, the fluorescent lifetimes would be affected.

**ELC purification:** **Figure 1** shows the steps and quality of purification. The top left image shows a Western blot using an anti-ELC antibody. The bottom left image shows a SDS gel stained with Sypro protein stain. Equivalent loading was performed for both the Western blot and the SDS gel. Lane 1 and lane 2 show the non-induced and induced cell lysate, respectively, indicating LC1 was being expressed by the bacterial system and identified by the ELC antibody. Lanes 3 to 6 show the different steps in the purification of LC1, namely treatment with lysis buffer (lane 3), wash buffer (lane 4), and elution buffers (lanes 5 and 6). The purification was also quite clear after column chromatography (lanes 5 and 6), compared to just before loading the expressed sample onto the column (lane 2).

**Labeling of myosin and actin in cardiac myofibrils:** **Figure 2** shows confocal images of fluorescently-labeled cardiac myofibrils. Myosin in myofibrils was exchanged with Rh-LC1 (**A**), AlexaATP (**B**), and Rh-phalloidin (**C**) as described in the Methods section. The degree of labeling was ~3-5% for Rh-LC1. The microscope had no trouble detecting such lightly labeled fibers.



Labeled ELC was exchanged with endogenous light chains into fibers as described earlier (84). Additionally, experiments were performed to verify that labeled light chains were actually exchanged into fibers when the endogenous protein was extracted out. The procedure is based on the fact that molecules can reversibly dissociate from their binding sites and be replaced by externally applied proteins competing for the free binding sites. Furthermore, the labeled exogenous protein specifically folds into the site due to its conformational affinity for the binding site. **Figure 3** demonstrates that the exchange successfully introduced fluorescent LC1 into muscle without extracting other proteins. The exchange consisted of SDS-PAGE of skeletal and cardiac muscle exchanged with fluorescent-light chains stained with Sypro Ruby protein stain (lanes 1-8). Lane 2 is a skeletal muscle fiber showing myosin (Myo), actin (Act) and light chains (LC1-3). After incubation for 0.50 hours at 30°C in essential light-chain exchange solution, lanes 2 and 3 for skeletal muscle and lanes 5 and 6 for cardiac muscle of the Sypro-stained gel of muscle are identical.

Earlier studies have demonstrated that TFP promotes extraction of native LC1 only when the LC1 is also added in the buffer exogenously (84). Thus, when the fiber is incubated in extraction buffer (which lacks exogenous LC1), LC1s are not dissociated from the heavy chain. When muscle is incubated for 0.5 hours at 30°C in exchange solution (identical to extracting solution but containing 1 mg/mL recombinant fluorescent LC1), again the Sypro staining shows no difference (refer to lanes 3 and 4 for skeletal muscle and lanes 6 and 7 for cardiac muscle). However, the fluorescent LC1 incorporates into skeletal (lane 12) and cardiac (lane 15) muscle. LC1 incorporates more efficiently

into skeletal than into cardiac muscle. Western blots using anti-LC1 antibody (lanes 17-23) identify fluorescent bands as LC1. This result proves that the exchange successfully introduces fluorescent LC1 into muscle. Incidentally, control experiments (not shown) revealed that if extracting solution contained no TFP, no exchange occurred.

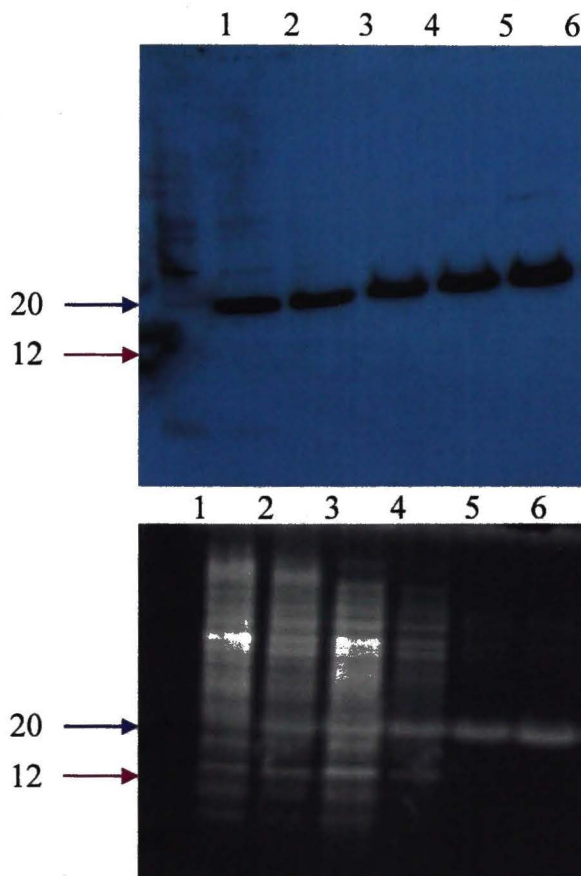


**Figure 1:** ELC purification: The top image is a Western blot using an anti-ELC antibody. The bottom left image is a Sypro protein stain. The arrow points to the expected size of LC1 (~20kDa)

Lane 1: Non-induced control

Lane 2: Cell lysate after induction with IPTG

Lane 3: Cleared cell lysate obtained after treatment with Lysis Buffer B to solubilize inclusion bodies

Lane 4: Flow-through collected after loading the Ni-NTA column with cleared cell lysate and washing the column with Wash Buffer C

Lane 5: Flow-through collected after loading the column with Elution Buffer D

Lane 6: Flow-through collected after loading the column with Elution Buffer E.

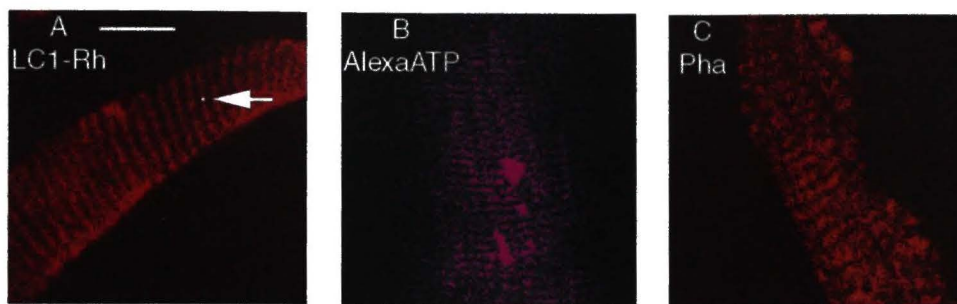


**Figure 2.** Confocal image of fluorescently labeled cardiac myofibrils. Myosin in myofibrils was exchanged with Rh-LC1 (A), AlexaATP (B), and Rh-phalloidin (C) as described in the Methods section. Muscle was illuminated with 568 nm light and viewed through 35  $\mu$ m pinhole and LP 590 (A & C) and Cy5 (B) filters. Bar=10  $\mu$ m. The round spot in A (pointed to by the arrow) shows the relative size of the illuminated spot in a Tg-wt muscle.

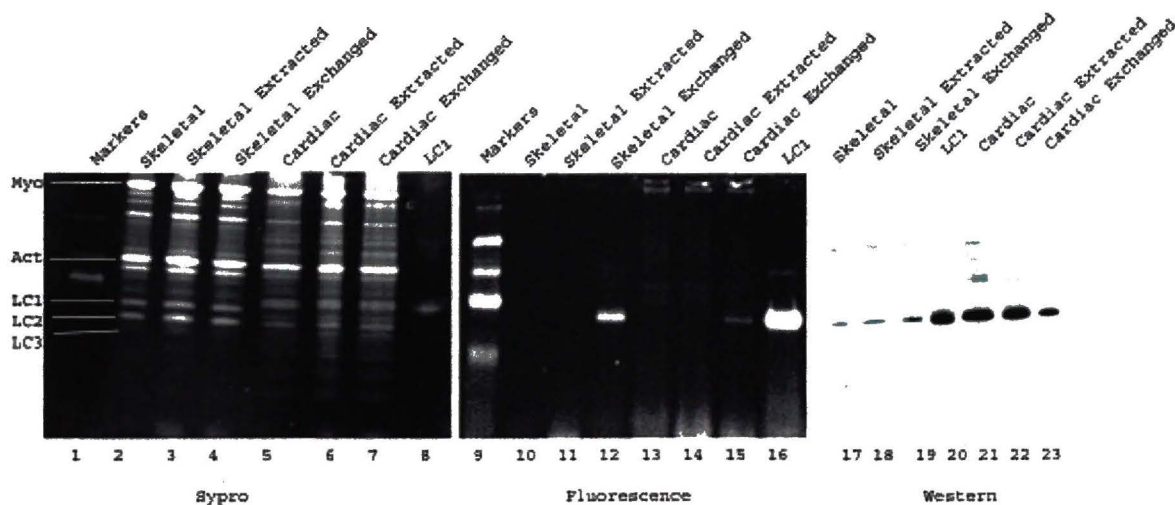


**Figure 3:** Incorporation of Rh-LC1 into skeletal and cardiac myofibrils. Incorporation of fluorescent light chains into muscle. Lanes 1-8 are SDS gels stained with Sypro Ruby protein stain. Lane 1: Protein markers 20KD, lane 2: rabbit psoas muscle fiber, lane 3: muscle fiber after incubation in extracting solution, lane 4: muscle fiber after incubation in exchanging solution containing recombinant, fluorescent LC1, lane 5: mouse cardiac muscle, lane 6: cardiac muscle after incubation in extracting solution, lane 7: muscle fiber after incubation in exchanging solution containing recombinant, fluorescent LC1, lane 8: recombinant LC1. Lanes 9-16 are fluorescent gels (before staining with Sypro) corresponding to lanes 1-8. Lanes 17-23 are Western blots stained with anti LC1 antibody. The samples are identified above each lane.



The motions of cross-bridges were synchronized by rapid (10 msec) photogeneration of ATP. During each 10 msec interval, all caged ATP is converted to ATP (14). Since the root-mean-square velocity of diffusion of ATP, determined by its diffusion coefficient ( $3.7 \times 10^{-6} \text{ cm}^2/\text{sec}$ , 40) is  $\sim 1 \text{ } \mu\text{m}/\text{msec}$ , it diffuses away from the experimental volume in  $\sim 300 \text{ } \mu\text{sec}$ . Therefore, after 300  $\mu\text{sec}$ , there is practically no free nucleotide left in the experimental volume, and the rates represent motion caused by the turnover of a single molecule of ATP.

**Cross-bridge dissociation from thin filaments:** Actin was labeled with Rh-Ph.

Dissociation was triggered by rapid generation of ATP from the caged precursor by shining a pulse of UV light at a small spot on the myofibril. Dissociation causes rotation of actin monomer, as it is no longer immobilized by myosin (10, 13). Muscle was initially in rigor. **Figure 4A** shows a typical record of perpendicular anisotropy change upon application of ATP. Upon rapid (10 msec) release of ATP from the cage (**Figure 4A**, arrow) anisotropy drops rapidly, indicating dissociation of cross-bridges from thin filaments. The time was measured by drawing the dissociation curve on an expanded time scale (**Figure 4B**) and estimating the time it took for anisotropy to decay from the maximum to a minimum.

**Table 1** summarizes the dissociation times ( $\tau_1$ ). Dissociation times were slightly higher in Tg-m fibers; the differences in  $\tau_1$  among the four groups were statistically significant ( $P = 0.0253$ ). Results show that cross-bridges of Tg-m (90%) muscle dissociate from thin filaments significantly more slowly than the cross-bridges of non-Tg



muscle ( $q = 3.813$ ,  $P \leq 0.05$ ). There were no significant differences in the rate of cross-bridge dissociation between the Tg-m (60%) and the non-Tg muscle.

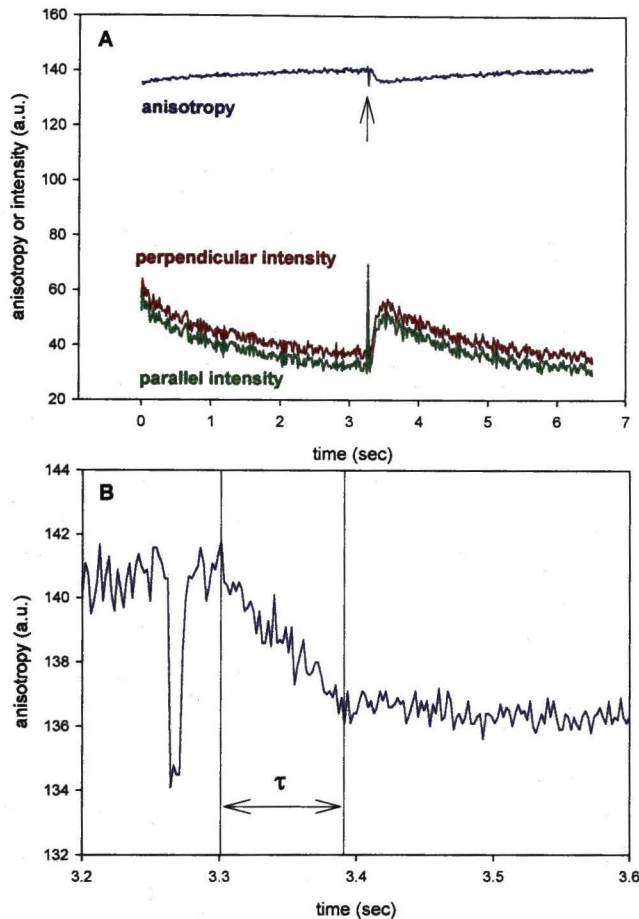


**Figure 4.** Time course of change of perpendicular anisotropy of muscle labeled with Rh-Ph. Muscle is initially in rigor. Sudden pulse applied at arrow generates ATP and causes single turnover of cross-bridges. **A)** Orthogonal intensities (red and green) and anisotropy (blue). “Parallel” and “perpendicular” refer to the orientation of polarization of linearly polarized fluorescent (emitted) light relative to the long axis of a myofibril. **B)** The drop in anisotropy indicates cross-bridge dissociation from thin filaments. The vertical lines were fitted by inspection. The distance between them is equal to the dissociation time.

Non-Tg (msec)	Tg-wt (msec)	Tg-m (E22K) (90%) (msec)	Tg-m (E22K) (60%) (msec)	Probe
165 ± 25* (n = 13)	172 ± 29 (n = 10)	210 ± 39* (n = 9)	200 ± 32 (n = 9)	Rh-Ph on actin

**Table 1.** Times of dissociation ( $\tau_1$ ) of cross-bridges from actin (as defined in **Fig. 4B**). The errors are standard deviations of  $n$  measurements. \*  $P \leq 0.05$  for Non-Tg vs. E22K (90%)

**Cross-bridge re-binding to thin filaments:** The rate of cross-bridge rebinding to actin,  $1/\tau_2$ , was determined from the rate of anisotropy change of the recombinant essential light chain of myosin labeled with rhodamine (Rh-LC1) exchanged for native LC1 in the cardiac myofibrils. Rebinding of cross-bridges to thin filaments was indicated by the slow exponential rise of anisotropy (**Figure 5**). The shape of anisotropy change of cardiac muscle was similar to skeletal muscle (10). The values of  $b$  ( $1/\tau_2$ ) are summarized in

**Table 2.** The differences in  $\tau_2$  among the four groups were statistically different ( $P = 0.04$ ). The results show that cross-bridges of Tg-m (90%) muscle rebind to thin filaments faster than the cross-bridges of non-Tg controls ( $q = 3.767$ ,  $P \leq 0.05$ ). Cross-bridges of Tg-wt muscle also rebind to thin filaments faster than the cross-bridges of non-Tg muscle ( $q = 3.623$ ,  $P \leq 0.05$ ). There were no significant difference in the rate of cross-bridge rebinding between the Tg-m (60%) and the non-Tg muscle.

**Table 2.** Rates of rotation ( $1/\tau_2$ ) of the myosin lever arm (mean  $\pm$  SD, as defined in Fig. 5B).

<b>Non-Tg</b> <b>(sec<sup>-1</sup>)</b>	<b>Tg-wt</b> <b>(sec<sup>-1</sup>)</b>	<b>Tg-m (E22K)(90%)</b> <b>(sec<sup>-1</sup>)</b>	<b>Tg-m (E22K) (60%)</b> <b>(sec<sup>-1</sup>)</b>	<b>Probe</b>
0.59 $\pm$ 0.19 <sup>γ§</sup> (n = 12)	1.10 $\pm$ 0.49 <sup>§</sup> (n = 11)	1.24 $\pm$ 0.90 <sup>γ</sup> (n = 15)	0.83 $\pm$ 0.34 (n = 9)	Rh-LC1

<sup>γ</sup>P < 0.05 for non-Tg vs. Tg-m

<sup>§</sup>P < 0.05 for non-Tg vs. Tg-wt

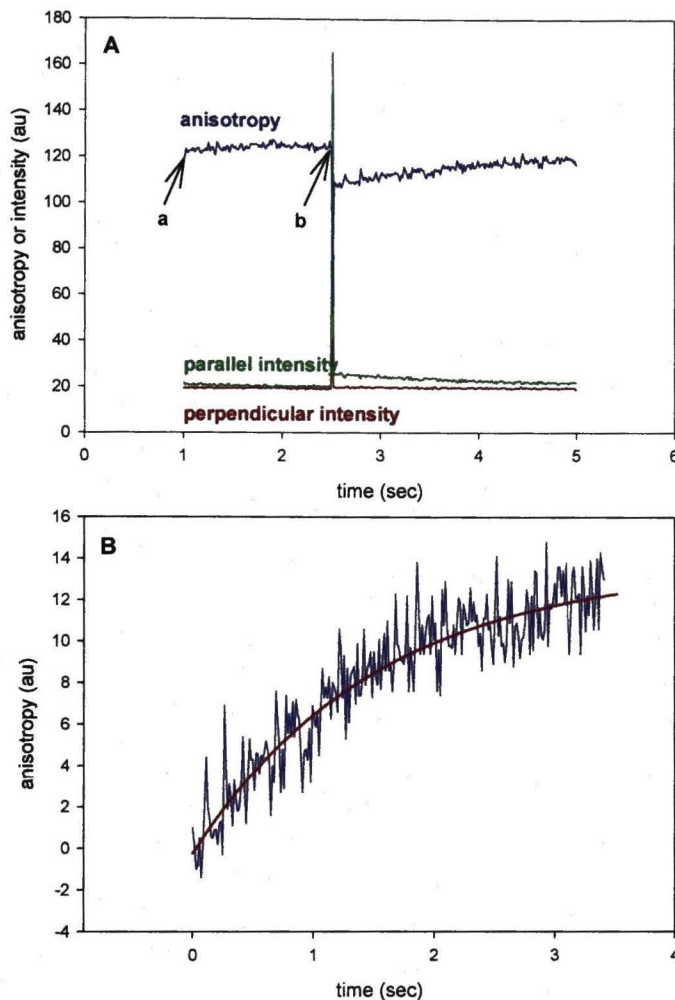


**Figure 5.** Time course of change of perpendicular anisotropy of muscle labeled with Rh-LC1. During the time interval from a to b, muscle is in rigor. A sudden pulse of UV light is applied at point b to release ATP and cause cross-bridges to undergo one turnover cycle. **A)** Orthogonal intensities and anisotropy **B)** The rise of anisotropy, indicates cross-bridge re-binding to thin filaments. To account for photobleaching, the anisotropy between points a and b was fitted to a curve and the anisotropy data subtracted from it. As a result, the “de-trended” data begins at 0. The data was fitted to an exponential rise to a maximum  $y = 107.8 + 13.9 (1 - e^{-0.65t})$ .

**Dissociation of ADP from the myosin active site:** Cross-bridges were labeled at the active site with Alexa-ADP. Upon sudden release of ATP, the cross-bridges dissociated from thin filaments. Fluorescent ADP was displaced from the myosin active site by the



rapidly photogenerated excess of non-fluorescent ATP. **Figure 6A** shows a typical record of perpendicular anisotropy change upon application of ATP to Tg-wt myofibrils. The shape of the anisotropy change of cardiac muscle was similar to that of skeletal muscle (10). Correction for photobleaching was performed as described in **Figure 5B**. A typical corrected curve is shown in **Figure 6B**. The dissociation time ( $\tau_3$ ) was estimated from this corrected anisotropy as illustrated in the figure. The dissociation time  $\tau_3$  for the three groups is summarized in **Table 3**. Results revealed that there were no statistically significant differences in the ADP dissociation times among the three groups ( $P = 0.6226$ ). The difference between  $\tau_1$  and  $\tau_3$  was not statistically significant. This is consistent with the fact that the dissociation of cross-bridges from actin occurs simultaneously with release of ADP in skeletal muscle (78).

**Table 3.** Times of ADP Dissociation ( $\tau_3$ ) from Myosin Active Site (mean  $\pm$  SD)

<b>Non-Tg</b> <b>(msec)</b>	<b>Tg-wt</b> <b>(msec)</b>	<b>Tg-m (E22K) (90%)</b> <b>(msec)</b>	<b>Probe</b>
102.5 $\pm$ 38.8  (n = 14)	117.0 $\pm$ 43.4  (n = 14)	131.3 $\pm$ 56.5  (n = 16)	Alexa ATP  on myosin

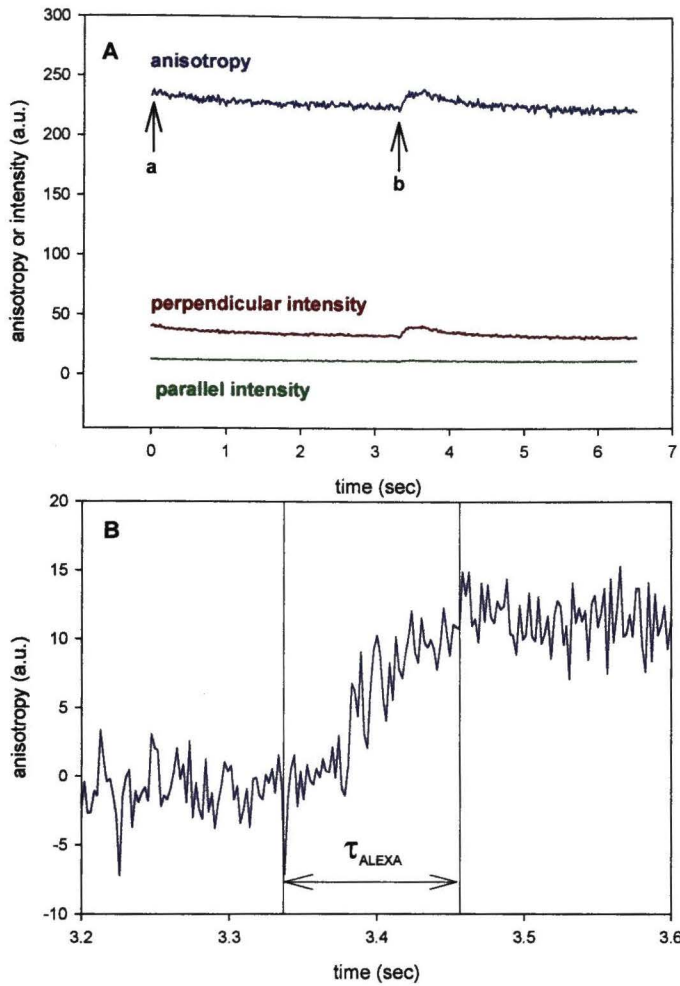


**Figure 6.** Time course of change of perpendicular anisotropy of muscle labeled with AlexaATP. Muscle is in rigor during the time interval from a to b. A sudden pulse applied at point b generates ATP and causes contraction. **A)** Orthogonal intensities and anisotropy. **B)** The rise of anisotropy, indicates ADP dissociation from the active site of myosin. To account for photobleaching, the anisotropy between points a and b was fitted to a curve and the anisotropy data subtracted from it. The vertical lines were fitted by inspection. The distance between them is equal to the dissociation time.

## 2. Cardiac Proteins *In Vitro*

Fluorescent Lifetimes: The fluorescent lifetimes were measured to test whether the Tg-m myosin is intrinsically different from the Tg-wt myosin. To do so fluorescein-phalloidin was attached to G-actin to which myosin was bound. Fluorescent lifetime is a precise measure of conformational change because it is very sensitive to environmental changes (48). If the mutation altered binding characteristics of myosin, the fluorescent lifetime of fluorescein on actin would be affected. **Figure 7** shows typical time-resolved fluorescence decay of phalloidin on actin (phalloidin : actin ratio = 1). The best fit was achieved using two lifetimes, the fast lifetime and the slow lifetime, with values of  $1.420 \pm 0.017$  ns and  $3.592 \pm 0.015$  ns respectively. Upon binding of equimolar Tg-wt myosin, the fast lifetime ( $1.420 \pm 0.017$  ns) increased by 0.7% to  $1.431 \pm 0.037$  ns and the slow lifetime did not change at all.

Similarly, binding of equimolar Tg-m to actin did not significantly change either lifetime. The complete analysis is shown in **Table 4**. Changes in both fast and long lifetime values were smaller than the standard deviation of measurement. In an effort to measure change in binding consistently, similar measurements were performed at the molar ratio of actin to myosin ranging from 0.5 to 2.5. In each case, no change in lifetime was observed. Thus the mutation does not cause differences in the affinity of myosin for actin. Together with the fact that the ATPase activity of Tg-m is the same as the ATPase activity of Tg-wt myosin, it can be concluded that mutation does not cause differences in the major properties of myosin.

It is possible that the observed changes of the anisotropy of the lever arm do not reflect rotation at all but instead reflect changes of anisotropy of the probe due to either (i) binding of cross-bridges to thin filaments, or (ii) ATP-mediated release of LC1 from the lever arm. To check for possibility (i), we compared the excitation anisotropies of solutions of Rh-LC1 incorporated into myosin with the anisotropy of actin-Rh-LC1-myosin complex (**Figure 8**). The limiting anisotropy of immobilized Rh-LC1-myosin (■) at 540 was 0.364. The anisotropy of Rh-LC1 bound to myosin in the absence of actin (●) at 540 nm was 0.289. Since myosin at low ionic strength is filamentous and does not execute any nanosecond-time-scale motions, this decrease indicates the collective motion of the probe and of myosin-bound light chain. The addition of increasing concentrations of actin (the colored circles) made no difference to the anisotropy. This suggests that it is unlikely that the observed anisotropy change is due to actin dissociation.

In principle, it is possible that the anisotropy remains unchanged due to compensating changes in the rotational correlation time of rhodamine and the fluorescence lifetime of rhodamine (Perrin's equation). However, this did not occur in this experiment; the fluorescence lifetimes in the absence and presence of actin were the same (**Table 4**). This proves that the anisotropy of Rh is unaffected by the formation of actomyosin complex and that the anisotropy change observed in fibers reflected the rotation of the lever-arm.

To check for possibility (ii), we compared excitation anisotropies of Rh-LC1-S1 in the presence and absence of ATP. Addition of 2 mM ATP to 0.5  $\mu$ M S1 exchanged



with Rh-LC1 made little difference to excitation anisotropy between 500 and 530 nm and no difference to anisotropy at 540 nm (**Figure 8B**, compare ● and ●).

Incidentally, the limiting anisotropy of immobilized Rh-LC1-myosin (**Figure 8A**) and Rh-LC1-S1 (**Figure 7B**) at 540 was 0.364 and 0.371, respectively. This translates to an angle of  $\sim 13^\circ$  between absorption and emission dipoles of rhodamine, which is consistent with earlier work (13).

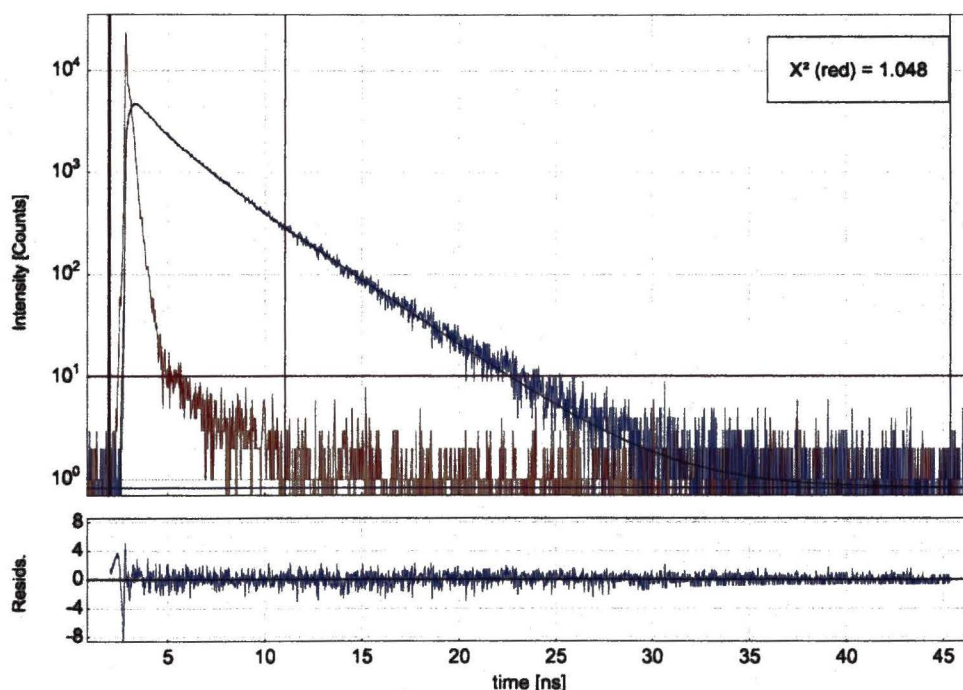


**Figure 7.** Fluorescent lifetime of fluorescein-phalloidin labeled 0.2  $\mu\text{M}$  actin. The blue line indicates the decay of fluorescence after excitation with 470 nm light pulse (red). The autocorrelation of the differences between the data and the fit (black line) is at the bottom. A total of 10826 data points were analyzed.

**Table 4.** Fluorescent excited state lifetimes ( $\tau_1$  and  $\tau_2$ ) of binding of Tg-wt and E22K myosin to actin. The top and bottom tables report changes after the binding of equimolar Tg-wt myosin and equimolar E22K myosin, respectively. The  $f_{\text{Intensity}}$  and  $f_{\text{Amplitude}}$  are the percentages of the total signal intensity and amplitude contributed by the processes decaying with lifetimes  $\tau_1$  and  $\tau_2$ .

Actin alone	Mean	SD	$f_{\text{Intensity}}$	$f_{\text{Amplitude}}$
$\tau_1$ (ns)	1.420	0.017	34.73	57.35
$\tau_2$ (ns)	3.592	0.015	65.27	42.65
Actin+Tg-wt	Mean	SD	$f_{\text{Intensity}}$	$f_{\text{Amplitude}}$
$\tau_1$ (ns)	1.431	0.018	34.36	56.80
$\tau_2$ (ns)	3.593	0.017	65.64	43.20

Actin alone	Mean	SD	$f_{\text{Intensity}}$	$f_{\text{Amplitude}}$
$\tau_1$ (ns)	1.400	0.017	36.37	59.34
$\tau_2$ (ns)	3.580	0.017	63.63	40.66
Actin+E22K	Mean	SD	$f_{\text{Intensity}}$	$f_{\text{Amplitude}}$
$\tau_1$ (ns)	1.408	0.018	35.74	58.60
$\tau_2$ (ns)	3.582	0.018	64.26	41.40

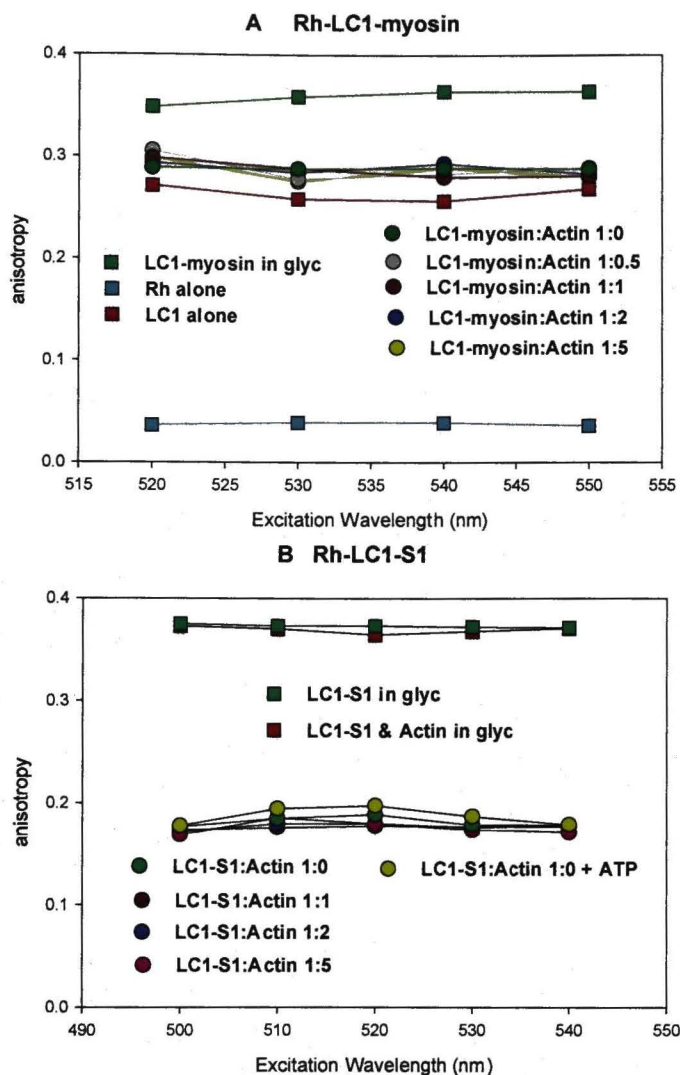


**Figure 8.** Excitation anisotropy of Rh-LC1. **A** shows the anisotropy of Rh-LC1-myosin in the absence of actin (●) compared with the anisotropy measured in the presence of increasing molar excesses of actin (0.5 [●], 1 [●], 2 [●], 5 [●] and 10 [●]). The anisotropy of Rh-LC1 exchanged to myosin and immobilized in 90% glycerol at 0°C (■) and free Rh-LC1 and free Rh (■) are shown as controls. 0.27  $\mu$ M myosin in 0.2 M KCl, 2 mM MgCl<sub>2</sub>, 0.1 mM CaCl<sub>2</sub>, and 10 mM KPi at pH = 7.5. All measurements were taken at 0°C. The excitation and emission slits were 1 mm,  $\lambda_{em}$  = 567 nm. **B** shows the anisotropy of Rh-LC1-S1 in the absence of actin (●) compared to the anisotropy measured in the presence of 1 (●), 2 (●), and 5 (●) molar excesses of actin. The anisotropy of Rh-LC1 measured in the absence (●) and presence (●) of 2 mM ATP is identical at and above 540 nm. 0.5  $\mu$ M myosin in 50 mM KCl, 2 mM MgCl<sub>2</sub>, 0.1 mM CaCl<sub>2</sub>, and 10 mM KPi at pH = 7.5. All measurements were taken at 20°C. The excitation and emission slits were 1 mm,  $\lambda_{em}$  = 567 nm.

## CHAPTER V

### DISCUSSION

The overall goal of this study was to understand how the E22K-RLC mutation affects muscle contraction by studying the kinetics of the cross-bridge cycle during force generation. This is the first study that has investigated the functional consequences of any RLC mutation at the molecular level using muscle obtained from a transgenic animal model. Assessing the mechanisms by which this mutation alters RLC function will lead to a better understanding of the physiological role of RLC in the regulation of cardiac muscle contraction. To this end, the enzymatic and mechanical events were followed in a small population of cross-bridges in working muscle. The mechanical events were measured by anisotropy of F-actin labeled with Rh-Ph and myosin labeled at the lever arm with Rh-LC1. The enzymatic events were followed by measuring the dissociation of ADP from the active site.

It is important to study and characterize the motion of cross-bridges in working muscle because the behavior of proteins *in vivo* may be different than their behavior *in vitro*. Molecular crowding influences protein solubility and conformation in solution (56). The effect of crowding is particularly severe in muscle, where actin and myosin are present at concentrations of hundreds of  $\mu\text{M}$  (7). Actin and myosin are meant to operate in such crowded environments, reflected by the fact that their  $K_m$  is in the  $\mu\text{M}$  range, but crowding may impose constraints affecting both the structure and function of enzymes so that their properties in dilute solutions are different than in muscle (3).



The experiments were performed on skeletal and cardiac muscle. The experiments on skeletal muscle were conducted primarily to establish our experimental approach; skeletal fibers have a simpler organization and are thus more amenable to biochemical manipulations such as labeling with a fluorescent probe. The rate of cross-bridge dissociation and rebinding measured in skeletal fibers was consistent with the previous work from our lab (10, 12, 13, 14).

In order to examine whether the point mutation in RLC leads to changes in cross-bridge kinetics, we followed the mechanical and enzymatic events in cardiac muscle from transgenic mice expressing the E22K mutation of myosin RLC. The measurements were performed on a very small area of muscle so as to follow the cross-bridge kinetics of minimal number of myosin heads in contracting cardiac myofibrils. Characterization of the motion of a small population of cross-bridges in working muscle is essential because the signal measuring the change in cross-bridge kinetics is not averaged over a large population of myosin heads.

Our investigation showed that the E22K mutation had a slight influence on the time of cross-bridge dissociation. This mutation resulted in an increase in the time of cross-bridge dissociation,  $\tau_1$ , for Tg-m (90%) myofibrils. The difference was not statistically significant with 60% of the myosin molecules carrying the mutation ( $P \geq 0.05$ ,  $q = 2.860$ ) but significant with 90% of the myosin ( $P \leq 0.05$ ,  $q = 3.813$ ). It is unlikely that this disparity reflects intrinsic differences in the binding of mutated myosin to actin; isolated Tg-m myosin bound to actin with the same affinity as isolated Tg-wt myosin. This, together with the fact that mutated and wild-type myosin have the same ATPase

activity (87), suggests that the observed difference in  $\tau_1$  is not due to intrinsic differences in cross-bridges but to hypertrophic abnormalities present in the transgenic hearts (87).

We observed no effect on the rate of cross-bridge re-binding to thin filaments. Control experiments were performed to confirm that the anisotropy changes reflected a rotation of the lever arm and not changes in the fluorescent-dipole movement of the probe. Movement of the probe could be attributed to changes in the environmental milieu by either the binding of cross-bridges to thin filaments or the ATP-mediated release of LC1 from the lever arm. Although the anisotropy of free Rh-LC1 (0.256 at 540 nm, ● in **Fig. 8A**) was increased to 0.289 for Rh-LC1-myosin in the absence of actin (● in **Fig. 8A**), suggesting that rotation of LC1 on myosin is restricted by the interactions with the heavy chain, it is unlikely that this interaction is loosened by ATP. The anisotropy of Rh-LC1 on S1 was unaffected by 2 mM ATP (**Fig. 8B**). The same was true of the anisotropy of Rh-LC1 on myosin. This lack of effect is consistent with the fact that loosening of LC1 from myosin requires high [ATP] or trifluoroperazine at a high temperature (80).

Finally, the mutation had no observable effect on the time of ADP dissociation from the myosin active site. The absolute values of cross-bridge dissociation and re-binding as well as ADP release reported in this experiment are lower than those observed in solution (100). This is because single-turnover experiments were performed to measure cross-bridge kinetics in this study. In a single turnover experiment, the cross-bridge detaches and reattaches only once; therefore, after reattaching, the probability of detachment becomes 0.

## **1. Possible Limitations of the Study**

1. Our results did not show any significant differences in cross-bridge kinetics between Tg-wt and Tg-E22K mice, showing that the presence of E22K-RLC mutation did not produce changes in the cross-bridge kinetics and the rate of ADP dissociation. It is possible that the Tg-E22K mice did not completely recapitulate the human phenotype of E22K-mutated hearts. While the Tg-E22K mice used in our study did show enlarged inter-ventricular septa and papillary muscles, the histopathological examination did not reveal any myofibrillar disarray (87).

Surprisingly, ECG did not show any significant differences in Tg-E22K mice. The left ventricular chamber dimensions in systole and diastole, ejection, or shortening fractions were similar in all animals. In addition, the heart weight to body weight ratios did not indicate cardiac hypertrophy in Tg-E22K mice. Thus the human phenotype of septal and papillary muscles hypertrophy observed in patients harboring this mutation (43, 67) was seen only qualitatively in the slides of whole hearts of Tg-E22K mice. It is possible that there were abnormalities in the ECG, but these abnormalities were not detected because the technology used to measure them is old. Perhaps the use of newer echocardiogram technology developed specifically for small animals could help in the future.

2. Another reason for not observing any differences in the cross-bridge kinetics could be the age of the mice used in our study. The transgenic mice used in our study varied in age between six and nine months. It has been shown in human patients that the older



members of a three-generation family carrying the mutation showed moderate hypertrophy of the entire septum, whereas the younger members had only mild or basal septal hypertrophy (43).

However, our collaborators in a previous study with the same breed of transgenic mice did not observe any age-dependent effects on hypertrophy. They utilized hearts from nine-month-old and 13-month-old mice and observed similarly enlarged inter-ventricular septa as well as papillary muscles (87). However, a recent study with mice expressing I79N-TnT mutation has demonstrated that mice developed hypertrophic phenotype between 15 and 20 months of age (6). Thus it is possible that the animals under study were too young to demonstrate the hypertrophic phenotype.

3. Our study measured the cross-bridge kinetics in the absence of load whereas the heart works under load *in-vivo*. In order to simulate *in-vivo* conditions an experimental system where the cardiac muscle is subjected to isometric tension to mimic the *in-vivo* state with the simultaneous measurement of cross-bridge kinetics can be devised.

4. The Tg hearts were observed to have a significantly different kinetics of lever arm re-binding than non-Tg hearts. There can be two reasons for this observation: First, while tension is an average of contributions from large populations of cross-bridges, each cross-bridge has different kinetics depending on its position relative to the actin-binding site (25). A consequence of this fact is that kinetics of a single cross-bridge may be different from kinetics of the whole assembly. If a single cross-bridge were monitored, the anisotropy of the lever-arm would be expected to change in four discrete steps, corresponding to cross-bridge release from actin, free rotation, weak binding, and



transition to the strongly-bound state. However, if the number of cross-bridges is large, these steps become obscured and their kinetics becomes altered. In our experiment the number of cross-bridges was estimated to be 400. The tension response, being an average of trillions of cross-bridges in a muscle bundle, can be quite different than the response of a few hundred myosin heads.

The second reason for the difference may be simply that non-transgenic mice express endogenous mouse RLC, while the transgenic mice (either wild-type or E22K-modified) express human RLC. There is a 95% homology between human ventricular RLC and murine ventricular RLC. Of the eight amino acids which are different between the human ventricular RLC and mice ventricular RLC, six are located in the N-terminal region of the RLC (at positions 4, 5, 10, 11, 13, and 14). The N-terminal domain wraps around the C-terminus of the myosin heavy chain. It is likely that any structural alterations in this N-terminal region of myosin would produce differences in the rate of the rotation of the lever arm.

## **2. Future Directions**

1. Chronic swimming exercise has previously been shown to exacerbate the pathologic phenotype of mice expressing FHC-linked mutation (34). A recent study evaluated the effects of FHC-causing troponin T mutations in transgenic mice when they were subjected to strenuous exercise (37). These mice were shown to have increased  $\text{Ca}^{2+}$  sensitivity of ATPase and force, similar to the E22K transgenic mice used in our studies.

While the chronic exercise did not result in significant histopathological changes, the F110I and I79N mice demonstrated a significant reduction of maximal exercise tolerance.

The authors hypothesized that exercise resulted in lowered pH and that the F110I and I79N mutations decreased the protective effect to changes in pH on the  $\text{Ca}^{2+}$  sensitivity. Large shifts in the  $\text{Ca}^{2+}$  sensitivity of force upon lowering the pH during cardiac muscle contraction is thought to protect the muscle when the heart undergoes potential strenuous exercise and/or ischemic injury. The authors performed reconstitution experiments utilizing human cardiac muscle preparations to test this theory. The experiments showed that when compared to the Wt-reconstituted fibers, the F110I- and I79N-reconstituted fibers showed significant decreases in  $\text{Ca}^{2+}$  sensitivity of force upon the lowering of the pH. These results suggest a mutant-related deficiency in the putative adaptive mechanism of cardiac muscle to lower pH. Since  $\text{Ca}^{2+}$  has been known to affect force development and cross-bridge kinetics, it is possible that cross-bridge kinetics is altered due to long- term strenuous exercise. Similar to the F110I- and I79N-TnT mutations, the E22K-RLC mutation also increases  $\text{Ca}^{2+}$  sensitivity of force and ATPase. It would be beneficial to discover the effect of strenuous chronic exercise on calcium sensitivity and cross-bridge kinetics.

2. A recent study (98) in transgenic mice expressing N47K-RLC and R58Q-RLC mutations has observed prolonged  $[\text{Ca}^{2+}]$  transients for both mutations. Prolonged  $[\text{Ca}^{2+}]$  transients in human patients carrying this mutation could lead to incomplete relaxation of the muscle during diastole, especially at high heart rates when the interval between  $[\text{Ca}^{2+}]$  transients becomes very short. This could happen under strenuous exercise conditions. A

short diastolic interval would increase diastolic  $[Ca^{2+}]$  as some amount of  $[Ca^{2+}]$  from the previous transient would still remain. This would lead to incomplete relaxation of the myocardium leading to incomplete filling of the myocardium, eventually resulting in a smaller stroke volume. In order for the myocardium to compensate, the heart rate would increase to maintain the cardiac output, resulting in an increased workload. This increased energy consumption could lead to myocardial hypertrophy over a long period of time.

The presence of prolonged  $[Ca^{2+}]$  transients has lead the researchers to believe that the  $[Ca^{2+}]$  binding site on RLC acts as a delayed  $[Ca^{2+}]$  buffer, much like parvalbumin, which functions as a delayed  $[Ca^{2+}]$  buffer in skeletal muscle (43). A recent study has demonstrated that over-expression of parvalbumin in cardiac myocytes from aged-rat myocardium was able to reverse age-related diastolic dysfunction (58). Thus the role of the  $Ca^{2+}$ -binding site on RLC was to act as a delayed  $[Ca^{2+}]$  buffer and shorten the  $[Ca^{2+}]$  transient by uptake of myoplasm  $[Ca^{2+}]$ , reducing intracellular  $[Ca^{2+}]$  (98).

Both the N47K- and R58Q-RLC mutations are similar to the E22K mutation in that they show increases in  $Ca^{2+}$  sensitivity of ATPase and steady-state force. While in E22K-RLC mutation  $Ca^{2+}$ -binding affinity is reduced 17 fold, the N47K and R58Q mutations result in the absence of  $Ca^{2+}$  binding (**Table 4, Chapter I**). Thus it is possible that the E22K-RLC mutation has a similar effect on  $Ca^{2+}$  transients. The binding of  $Ca^{2+}$  to RLC may help myosin in detecting  $[Ca^{2+}]_i$ , and thus help in modulating cross-bridge kinetics accordingly. The FHC-RLC mutations near the  $Ca^{2+}$ -binding site reduce or



eliminate  $\text{Ca}^{2+}$  binding, which reduces the ability of myosin to modulate cross-bridge kinetics based on the  $\text{Ca}^{2+}$  levels.

3. It is important to investigate as few molecules at a time as possible because each myosin head has its own rate of cross-bridge dissociation, rebinding, and ATP hydrolysis. The kinetics of orientation can be lost when the signal is coming from too many cross-bridges. When studying one cross-bridge, each step of the cross-bridge cycle is seen to be clearly differentiated; when studying 50 cross-bridges, some intermediate states can be seen; when studying 400 cross-bridges, some information is lost; and when studying 1,000 cross-bridges, much information is lost. We have studied an average of 400 cross-bridges at time using our current technique of data collection. New technologies are being developed which will allow us to study as few cross-bridges as possible at a time, and in the future it will be possible to study a single cross-bridge.

One technique with which our lab is currently working is the use of silver-island films to enhance fluorescence by decreasing photobleaching and enhancing emissions. The technique results in a smaller volume still sufficient to generate data, which effectively means a smaller number of cross-bridges, than that used in this study. Another technology currently being developed is surface-plasmon fluorescence, in which a glass cover slip is coated with a thin metal film to enhance the light impinging on the muscle. The resulting smaller experimental volume can be used to generate data.

4. It would also be beneficial to study the cross-bridge kinetics of N47K and R58Q mutations in the recently developed transgenic mice expressing these mutations. Binding to  $\text{Ca}^{2+}$  is eliminated in both of these mutations. In reconstituted muscle preparations of



these mice, increased  $\text{Ca}^{2+}$  sensitivity of ATPase and force and decreased steady-state force was observed.

## CHAPTER VI

### CONCLUSION

This study examined transgenic mouse cardiac myofibrils during single-turnover contraction to examine the influence of E22K mutation on (i) dissociation time,  $\tau_1$ , of myosin heads from thin filaments, (ii) re-binding time,  $\tau_2$ , of the cross-bridges to actin, and (iii) the dissociation time,  $\tau_3$ , of ADP from the active site of myosin. Dissociation time ( $\tau_1$ ) was determined from the increase in the rate of the rotation of the actin monomer when the myosin head was detached from the thin filaments during the cross-bridge cycle (c). Re-binding time ( $\tau_2$ ) was determined from the rate of change in anisotropy when the native LC1 in cardiac myofibrils was exchanged for the recombinant LC1 labeled with rhodamine. Dissociation time ( $\tau_3$ ) was determined from the anisotropy of muscle pre-loaded with a stoichiometric amount of fluorescent ADP. This ADP starts rotating rapidly once it is released from immobile myosin by sudden release of excess non-fluorescent ATP. The cross-bridges were induced to undergo a single detachment-attachment cycle by a precise delivery of stoichiometric ATP from a caged precursor. The times were measured in transgenic-mutated (Tg-m) heart myofibrils overexpressing the E22K mutation of human cardiac RLC. Transgenic wild-type (Tg-wt) and non-transgenic (non-Tg) muscles acted as controls.  $\tau_1$  was statistically greater in Tg-m than in the controls.  $\tau_2$  was less in Tg-m than non-Tg but the same as Tg-wt.  $\tau_3$  was the same in Tg-m and in the controls.

In an effort to see if observed differences in  $\tau_1$  were due to intrinsic differences in myosin, the binding of Tg-m and Tg-wt myosin to fluorescently-labeled actin was measured. No differences in binding were observed. The main conclusion which can be drawn from this study is that the E22K mutation has no effect on the cross-bridge kinetics of the cardiac muscle from transgenic mice carrying the E22K-RLC mutation. This could be because the Tg-E22K mice did not completely recapitulate the human phenotype of E22K-mutation. While the Tg-E22K mice used in our study did show enlarged inter-ventricular septa and papillary muscle, myofibrils did not display any disarray and the ECG also did not display any abnormalities. The slight increase in  $\tau_1$  was probably caused by myofibrillar disarray. The decrease in  $\tau_2$  of Tg hearts was probably caused by replacement of the mouse RLC for the human isoform in the transgenic mice.

## REFERENCES

1. **Allen TS, Ling N, Irving M, and Goldman YE.** Orientation changes in myosin regulatory light chains following photorelease of ATP in skinned muscle fibers. *Biophys J*, 70: 1847-1862, 1996.
2. **Andersen PS, Havndrup O, and Bundgaard H.** Myosin light chain mutations in familial hypertrophic cardiomyopathy: phenotypic presentation and frequency in Danish and South African populations. *J Med Genet*, 38: E43-E45, 2001.
3. **Arakawa T and Timasheff SN.** Theory of protein solubility. *Methods Enzymol*, 114: 49-77, 1985.
4. **Araujo A and Walker JW.** Kinetics of tension development in skinned cardiac myocytes measured by photorelease of  $\text{Ca}^{2+}$ . *Am J Physiol*, 267: H1643-H1653, 1994.
5. **Ashrafian H, Redwood C, Blair E, and Watkins H.** Hypertrophic cardiomyopathy: a paradigm for myocardial energy depletion. *Trends in Genetics*, 19: 263-268, 2003.
6. **Aziz T, Perrotta L, Knollmann BE, Weissman NJ, Potter JD, and Knollmann, BC.** Characterization of Troponin T Dilated Cardiomyopathy Mutations in the Fetal Troponin Isoform. *J. Biol. Chem*, 280: 17584-17592, 2005.
7. **Bagshaw CR.** *Muscle Contraction*. London: Chapman & Hall, 1982.
8. **Berger CL, Craik JS, Trentham DR, Corrie JE, and Goldman YE.** Fluorescence polarization of skeletal muscle fibers labeled with rhodamine isomers on the myosin heavy chain. *Biophys J*, 71: 3330-3343, 1996.
9. **Bonne G, Carrier L, Richard P, Hainque B, and Schwartz K.** Familial hypertrophic cardiomyopathy: from mutations to functional defects. *Circ Res*, 83: 580-593, 1998.
10. **Borejdo J and Akopova I.** Orientational Changes of Cross-Bridges During Single Turnover of ATP. *Biophys J*, 84: 2450-2459, 2003.
11. **Borejdo J and Putnam S.** Polarization of fluorescence from single skinned glycerinated rabbit psoas fibers in rigor and relaxation. *Biochem Biophys Acta*, 459: 578-595, 1977.
12. **Borejdo J, Shepard A, Dumka D, Akopova I, Talent J, Malka A, and Burghardt TP.** Changes in orientation of actin during contraction of muscle. *Biophys J*, 86: 2308-2317, 2004.
13. **Borejdo J, Shepard AA, Akopova I, Grudzinski W, and Malicka J.** Rotation of the lever-arm of myosin in contracting skeletal muscle fiber measured by two-photon anisotropy. *Biophys J*, 87: 3912-3921, 2004.
14. **Borejdo J, Ushakov DS, and Akopova I.** The essential light chains 1 and 3 rotate differently during muscle contraction. *Biophys J*, 82: 362a, 2002.



15. **Brenner B.** Effect of  $\text{Ca}^{2+}$  on cross-bridge turnover kinetics in skinned single rabbit psoas fibers: implications for regulation of muscle contraction. *Proc Natl Acad Sci USA*, 85: 3265–3269, 1988.
16. **Burghardt TP and Ajtai K.** Following the rotational trajectory of the principal hydrodynamic frame of a protein using multiple probes. *Biochemistry*, 33: 5376–5381, 1994.
17. **Butler TM, Siegman MJ, Mooers SU and Barsotti RJ.** Myosin light chain phosphorylation does not modulate cross-bridge cycling rate in mouse skeletal muscle. *Science*, 220: 1167–1169, 1983.
18. **Chaen S, Shirakawa I, Bagshaw CR, and Sugi H.** Measurement of nucleotide release kinetics in single skeletal muscle myofibrils during isometric and isovelocity contractions using fluorescence microscopy. *Biophys J*, 73: 2033–2042, 1997.
19. **Corrie JE, Brandmeier BD, Ferguson RE, Trentham DR, Kendrick-Jones J, Hopkins SC, van der Heide UA, Goldman YE, Sabido-David C, Dale RE, Criddle S, and Irving M.** Dynamic measurement of myosin light-chain-domain tilt and twist in muscle contraction. *Nature*, 400: 425–430, 1999.
20. **Cooke R, Franks K, and Stull JT.** Myosin phosphorylation regulates the ATPase activity of permeable skeletal muscle fibers. *FEBS Lett*, 144: 33–37, 1982.
21. **Crow MT, and Kushmerick MJ.** Myosin light chain phosphorylation is associated with a decrease in the energy cost for contraction in fast twitch mouse muscle. *J Biol Chem*, 257: 2121–2124, 1982.
22. **Davis JS, Hassanzadeh S, Winitzky S, Lin H, Satorius C, Vemuri R, Wen H, and Epstein ND.** The overall pattern of cardiac contraction depends on a spatial gradient of myosin regulatory light chain phosphorylation. *Cell*, 107: 631–641, 2001.
23. **Denk W, Piston DW, and Webb WW.** Two-Photon Molecular Excitation in Laser-Scanning Microscopy. In: *Handbook of Biological Confocal Microscopy*, edited by Pawley J. New York & London: Plenum Press, 1995.
24. **Dos Remedios CG, Millikan RG, and Morales MF.** Polarization of tryptophan fluorescence from single striated muscle fibers. A molecular probe of contractile state. *J Gen Physiol*, 59: 103–120, 1972.
25. **Dos Remedios CG, Yount RG, and Morales MF.** Individual states in the cycle of muscle contraction. *Proc Natl Acad Sci USA*, 69: 2542–2546, 1972.
26. **Eisenberg E, Hill TL, and Chen Y.** Cross-bridge model of muscle contraction. Quantitative analysis. *Biophys J*, 29: 195–227, 1980.
27. **Epstein ND.** The molecular biology and pathophysiology of hypertrophic cardiomyopathy due to mutations in the beta myosin heavy chains and the essential and regulatory light chains. *Adv Exp Med Biol*, 453: 105–114, 1998.
28. **Fatkin D, and Graham RM.** Molecular mechanism of inherited cardiomyopathies. *Physiol Rev*, 82: 945–980, 2002.

29. **Fitzsimons, DP, Bodell PW, and Baldwin KM.** Myocardial functional correlates of cardiac myosin light chain-2 phosphorylation. *J App Physiol*, 68: 2426–2433, 1990.
30. **Flavigny J, Richard P, Isnard R, Carrier L, Charron P, Bonne G, Forissier JF, Desnos M, Dubourg O, Komajda M, Schwartz K, and Hainque B.** Identification of two novel mutations in the ventricular regulatory myosin light chain gene (MYL2) associated with familial and classical forms of hypertrophic cardiomyopathy. *J Mol Med*, 76: 208-214, 1998.
31. **Goody RS.** The missing link in the muscle cross-bridge cycle. *Nature Struc Biol*, 10: 773-775, 2003.
32. **Gulick J, Hewett TE, Klevitsky R, Buck SH, Moss RL, and Robbins J.** Transgenic remodeling of the regulatory myosin light chains in the mammalian heart. *Circ Res*, 80: 655–664, 1997.
33. **Geisterfer-Lowrance AA, Kass S, Tanigawa G, Vosberg HP, McKenna W, Seidman CE, and Seidman JG.** A molecular basis for familial hypertrophic cardiomyopathy: a beta cardiac myosin heavy chain gene missense mutation. *Cell*, 62: 999-1006, 1990.
34. **Geisterfer-Lowrance AA, Christe M, Conner DA, Ingwall JS, Schoen FJ, Seidman CE, Seidman JG.** A Mouse Model of Familial Hypertrophic Cardiomyopathy. *Science*, 3: 272 (5262): 731-734, 1996.
35. **Goldman YE.** Wag the tail: structural dynamics of actomyosin. *Cell*, 93: 1-4, 1998.
36. **Goldman YE, Hibberd MG, and Trentham DR.** Initiation of active contraction by photogeneration of adenosine-5'-triphosphate in rabbit psoas muscle fibres. *J Physiol (Lond)*, 354: 605-624, 1984.
37. **Hernandez O, Szczesna-Cordary D, Knollman BC, Miller T, Bell M, Zhao J J, Sirenko, SG, Diaz Z, Guzman G, Xu Y, Wang Y, Kerrick WG, and Potter JD.** F110I and R278C Troponin T Mutations that Cause Familial Hypertrophic Cardiomyopathy Affect Muscle Contraction in Transgenic Mice and Reconstituted Human Cardiac Fibers. *J Biol Chem*, 280: 37183-37194, 2005.
38. **Highsmith S.** Lever Arm Model of Force Generation by Actin-Myosin-ATP *Biochemistry*, 38: 9791-9797, 1999.
39. **Highsmith S, Mendelson R, and Morales F.** Affinity of myosin S-1 for F-actin measured by time resolved fluorescence anisotropy. *Proc Nat. Aca. Sci USA*, 73: 1331-1337, 1976.
40. **Hubley MJ, Locke BR, and Moerland TS.** The effects of temperature, pH, and magnesium on the diffusion coefficient of ATP in solutions of physiological ionic strength. *Biochim Biophys Acta*, 1291: 115-121, 1996.
41. **Irving M, St Claire Allen T, Sabido-David C, Craik JS, Brandmeier B, Kendrick-Jones J, Corrie JE, Trentham DR, and Goldman YE.** Tilting of the light-chain region of myosin during step length changes and active force generation in skeletal muscle. *Nature*, 375: 688-691, 1995.
42. **James J, Zhang Y, Wright K, Witt S, Glascock E, Osinska H, Klevitsky R, Martin L, and Robbins J.** Transgenic rabbits expressing mutant essential light



- chain do not develop hypertrophic cardiomyopathy. *J Mol Cell Cardiol*, 34: 873-882, 2002.
43. **Johnson JD, Jiang Y, and Rall JA.** Intracellular EDTA mimics parvalbumin in the promotion of skeletal muscle relaxation. *Biophys J*, 76: 1514-1522, 1999.
  44. **Kabaeva ZT, Perrot A, Wolter B, Dietz R, Cardim N, Correia JM, Schulte HD, Aldashev AA, Mirrakhimov MM, and Osterziel KJ.** Systematic analysis of the regulatory and essential myosin light chain genes: genetic variants and mutations in hypertrophic cardiomyopathy. *Eur J Hum. Gene*, 10: 741-748, 2002.
  45. **Kimura A, Harada H, Park JE, Nishi H, Satoh M, Takahashi M, Hiroi S, Sasaoka T, Ohbuchi N, Nakamura T, Koyanagi T, Hwang TH, Choo JA, Chung KS, Hasegawa A, Nagai R, Okazaki O, Nakamura H, Matsuzaki M, Sakamoto T, Toshima H, Koga Y, Imaizumi T, and Sasazuki T.** Mutations in the cardiac troponin I gene associated with hypertrophic cardiomyopathy. *Nat Genet*, 16: 379-382, 1997.
  46. **Kubalak SW, Miller-Hance WC, O'Brien TX, Dyson E, and Chien KR.** Chamber specification of atrial myosin light chain-2 expression precedes septation during murine cardiogenesis. *J Biol Chem*, 269:16961-16970, 1994.
  47. **Kentish JC, Palmer S, and Lee JA.** Inactivation of the cardiac inotrope EMD 57033 by flash photolysis in isolated rat ventricular muscle. *J Physiol*, 475: 81-86, 1994.
  48. **Lakowicz JR.** *Principles of Fluorescence Spectroscopy*. New York & London: Plenum, Second Edition, 1999.
  49. **Levine RJ, Yang Z, Epstein ND, Fananapazir L, Stull JT, and Sweeney HL.** Structural and functional responses of mammalian thick filaments to alterations in myosin regulatory light chains. *J Struct Biol*, 122 (1-2): 149-161, 1998.
  50. **Ling N, Shrimpton C, Sleep J, Kendrick-Jones J, and Irving M.** Fluorescent probes of the orientation of myosin regulatory light chains in relaxed, rigor, and contracting muscle. *Biophys J*, 70: 1836-1846, 1996.
  51. **Lutucuta S, Tsybouleva N, Ishiyama M, DeFreitas G, Wei L, Carabello B, and Marian AJ.** Induction and reversal of cardiac phenotype of human hypertrophic cardiomyopathy mutation cardiac troponin T-Q92 in switch on-switch off bigenic mice. *J Am Coll Cardiol*, 44(11): 2221 - 2230, 2004.
  52. **Marian AJ, and Roberts R.** The molecular basis of hypertrophic cardiomyopathy. *Mol Cell Cardiol*, 33: 655-670, 2001.
  53. **Martin H, Bell MG, Ellis-Davies GCR, and Barsotti RJ.** Activation kinetics of skinned cardiac muscle by laser photolysis of nitrophenyl-EGTA. *Biophys J*, 86: 978-990, 2004.
  54. **Maughan DW.** Kinetics and energetics of the crossbridge cycle. *Heart Fail Rev*, 10: 175-185, 2005.
  55. **Metzger JM, Greaser ML, and Moss RL.** Variations in cross-bridge attachment rate and tension with phosphorylation of myosin in mammalian skinned skeletal muscle fibers. Implications for twitch potentiation in intact muscle. *J Gen Physiol*, 93: 855-883, 1989.

56. **Miller T, Szczesna D, Housmans P R, Zhao J, deFreitas F, Gomes AV, Culbreath L, McCue J, Wang Y, and Xu Y.** . Abnormal contractile function in transgenic mice expressing an FHC-Linked Troponin T (I79N) mutation. *J Biol Chem*, 276: 3743-3755, 2001.
57. **Minton AP.** Molecular crowding: analysis of effects of high concentrations of inert cosolutes on biochemical equilibria and rates in terms of volume exclusion. *Methods Enzymol*, 295: 127-149, 1998.
58. **Michele DE, Szatkowski ML, Albayya FP, and Metzger JM.** Parvalbumin gene delivery improves diastolic function in the aged myocardium in vivo. *Mol Therapy*, 10: 399-403, 2004.
59. **Morano I.** Tuning the human heart molecular motors by myosin light chains. *J Mol Med*, 77: 544-55, 1999.
60. **Mogensen J, Klausen IC, Pedersen AK, Egeblad H, Bross P, Kruse TA, Gregersen N, Hansen PS, Baandrup U, and Borglum AD.** Alpha-cardiac actin is a novel disease gene in familial hypertrophic cardiomyopathy. *J Clin Invest*, 103: R39-43, 1999.
61. **Mulvihill DP and Hyams JS.** Shedding a little light on light chains. *Nature Cell Biology*, 3: E1-E2, 2001.
62. **Muthuchamy M, Pieples K, Rethinasamy P, Hoit B, Grupp IL, Boivin GP, Wolska B, Evans C, Solaro RJ, and Wieczorek DF.** Mouse model of a familial hypertrophic cardiomyopathy mutation in alpha-tropomyosin manifests cardiac dysfunction. *Cir Res*, 85: 47-56, 1999.
63. **Nihei T, Mendelson, RA, & Botts, J.** Use of fluorescence polarization to observe changes in attitude of S1 moieties in muscle fibers. *Biophys J*, 14: 236-242, 1974.
64. **Pardee JD and Spudich JA.** Purification of muscle actin. *Methods Enzymol*, 85: 164-181, 1982.
65. **Palmiter KA, Tyska MJ, Dupuis DE, Alpert NR, and Warshaw DM.** Kinetic differences at the single molecule level account for the functional diversity of rabbit cardiac myosin isoforms. *J of Physiol*, 519: 669-678, 1999.
66. **Pemrick, SM.** The phosphorylated L2 light chain of skeletal myosin is a modifier of the actomyosin ATPase. *J Biol Chem*, 255: 8836-8841, 1980.
67. **Persechini A, Stull JT, and Cooke R.** The effect of myosin phosphorylation on the contractile properties of skinned rabbit skeletal muscle fibers. *J. Biol Chem*, 260: 7951-7954, 1985.
68. **Poetter K, Jiang H, Hassanzadeh S, Master SR, Chang A, Dalakas MC, Rayment I, Sellers JR, Fananapazir L, and Epstein ND.** Mutations in either the essential or regulatory light chains of myosin are associated with a rare myopathy in human heart and skeletal muscle. *Nat Genet*, 13: 63-69, 1996.
69. **Rayment I, Rypniewski W, Schmidt-Base K, Smith R, Tomchik DR, Benning MM, Winkelman DA, Wesenberg G, and Holden HM.** Three-dimensional structure of myosin subfragment-1: a molecular motor. *Science*, 261: 50-58, 1993.
70. **Richard P, Charron P, Carrier L, Ledeuil C, Cheav T, Pichereau C, Benaiche A, Isnard R., Dubourg O, and Burban M.** Hypertrophic cardiomyopathy:



- distribution of disease genes, spectrum of mutations, and implications for a molecular diagnosis strategy. *Circulation*, 107: 2227-2232, 2003.
71. **Roopnarine O.** Mechanical defects of muscle fibers with myosin light chain mutants that cause cardiomyopathy. *Biophys J*, 84: 2440-2449, 2003.
  72. **Roopnarine O, and Leinwand LA** Functional analysis of myosin mutations that cause familial hypertrophic cardiomyopathy. *Biophys. J*, 75: 3023-3030, 1998.
  73. **Sabido-David C, Brandmeier B, Craik JS, Corrie JE, Trentham DR, and Irving M.** Steady-state fluorescence polarization studies of the orientation of myosin regulatory light chains in single skeletal muscle fibers using pure isomers of iodoacetamidotetramethylrhodamine. *Biophys J*, 74: 3083-3092, 1998.
  74. **Sanbe A, Nelson D, Gulick J, Setser E, Osinska H, Wang X, Hewett TE, Klevitsky R, Hayes E, Warshaw DM, and Robbins J.** In vivo analysis of an essential myosin light chain mutation linked to familial hypertrophic cardiomyopathy. *Circ Res*, 87: 296-302, 2000.
  75. **Satoh M, Takahashi M, Sakamoto T, Hiroe M, Marumo F, and Kimura A.** Structural analysis of the titin gene in hypertrophic cardiomyopathy: identification of a novel disease gene. *Biochem Biophys Res Commun*, 262: 411-417, 1999.
  76. **Seidman JG, and Seidman C.** The genetic basis for cardiomyopathy: from mutation identification to mechanistic paradigms. *Cell*, 104: 557-567, 2001.
  77. **Shepard A and Borejdo J.** Correlation between mechanical and enzymatic events in contracting skeletal muscle fiber. *Biochemistry*, 43: 2804-2811, 2004.
  78. **Shepard AA, Dumka D, Akopova I, Talent J, and Borejdo J.** Simultaneous measurement of rotations of myosin, actin and ADP in contracting skeletal muscle fiber. *J Muscl Res Cell Mot*, 25: 549-557, 2004.
  79. **Shirakawa I, Chaen S, Bagshaw CR, and Sugi H.** Measurement of nucleotide exchange rate constants in single rabbit soleus myofibrils during shortening and lengthening using a fluorescent ATP analog. *Biophys J*, 78: 918-926, 2000.
  80. **Siemankowski RF, Wiseman MO, and White HD.** ADP dissociation from actomyosin subfragment-1 is sufficiently slow to limit the unloaded shortening velocity in vertebrate muscle. *Proc Natl Acad Sci*, 82: 658-662, 1985.
  81. **Sivaramakrishnan M and Burke M.** Studies on the subunit interactions of skeletal muscle myosin subfragment 1. Evidence for subunit exchange between isozymes under physiological ionic strength and temperature. *J Biol Chem*, 256: 2607-2610, 1981.
  82. **Solaro RJ, Pang DC, and Briggs FN.** The purification of cardiac myofibrils with Triton X-100. *Biochem Biophys Acta*, 245: 259-262, 1971.
  83. **Stepkowski, D, Szczesna D, Wrotek M, and Kakol I.** Factors influencing interaction of phosphorylated and dephosphorylated myosin with actin. *Biochim Biophys Acta*, 831: 321-329, 1985.
  84. **Sweeney HL.** Function of the N-terminus of the myosin essential light chain of vertebrate striated muscle. *Biophys J*, 68: 112s-119s, 1995.
  85. **Sweeney HL, and Kushmerick MJ.** Myosin phosphorylation in permeabilized rabbit psoas fibers. *Am J Physiol*, 249: C362-365, 1985.

86. **Sweeney HL, and Stull JT.** Alteration of cross-bridge kinetics by myosin light chain phosphorylation in rabbit skeletal muscle: implications for regulation of actin-myosin interaction. *Proc Natl Acad Sci. USA*, 87: 414-8, 1990.
87. **Szczesna D, Ghosh D, Li Q, Gomes AV, Guzman G, Arana C, Zhi G, Stull JT, and Potter JD.** Familial hypertrophic cardiomyopathy mutations in the regulatory light chains of myosin affect their structure,  $\text{Ca}^{2+}$  binding, and phosphorylation. *J Biol Chem* 276: 7086-7092, 2001.
88. **Szczesna-Cordary D, Guzman G, Zhao J, Hernandez O, Wei J, and Diaz-Perez Z.** The E22K mutation in myosin RLC that causes familial hypertrophic cardiomyopathy increases calcium sensitivity of force and ATPase in transgenic mice. *J Cell Sci*, 118: 3675-3683, 2005.
89. **Szczesna-Cordary D.** Regulatory light chains of striated muscle myosin: structure, function and malfunction. *Curr Drug Tar- Cardio and Haematol Dis*, 3: 187-197, 2003.
90. **Szczesna D, Zhao J, Jones M, Zhi G, Stull J, and Potter JD.** Phosphorylation of the regulatory light chains of myosin affects  $\text{Ca}^{2+}$  sensitivity of skeletal muscle contraction. *J Appl Physiol*, 92: 1661-1670, 2002.
91. **Szczesna-Cordary D, Guzman G, Ng SS, and Zhao J.** Familial hypertrophic cardiomyopathy linked alterations in  $\text{Ca}^{2+}$  binding of human cardiac myosin regulatory light chain affect cardiac muscle structure. *J Biol Chem*, 279: 3535-3542, 2004.
92. **Tanner JW, Thomas, DD, and Goldman, Y.E.** Transients in orientation of a fluorescent cross-bridge probe following photolysis of caged nucleotides in skeletal muscle fibers. *J Mol Biol*, 223: 185-203, 1992.
93. **Tardiff JC.** Sarcomeric proteins and familial hypertrophic cardiomyopathy: linking mutations in structural proteins to complex cardiovascular phenotypes. *Heart Fail. Rev*, 10: 237-248, 2005.
94. **Thierfelder L, Watkins H, MacRae C, Lamas R, McKenna W, Vosberg HP, Seidman JG, and Seidman CE.** Alpha-tropomyosin and cardiac troponin T mutations cause familial hypertrophic cardiomyopathy: a disease of the sarcomere. *Cell*, 77: 701-712, 1994.
95. **Thomas DD.** Spectroscopic probes of muscle cross-bridge rotation. *Ann Rev Physiol*, 49: 691-709, 1987.
96. **Tonomura Y, Appel P, and Morales MF.** On the molecular weight of myosin. II. *Biochemistry*, 5: 515-521, 1966.
97. **Tsoutsman T, Lam L, and Semsarian C.** Genes, calcium and modifying factors in hypertrophic cardiomyopathy. *Clin and Exp Pharmac and Physiol*, 33: 139-140, 2006.
98. **Wang, Y, Xu, Y, Kerrick G, Wang Y, Guzman G, Diaz-Perez Z, and Szczesna-Cordary D.** Prolonged  $\text{Ca}^{2+}$  and force transients in myosin RLC transgenic mouse fibers expressing malignant and benign FHC mutations *J. Mol Biol*, 361: 286-289, 2006.

99. **Watkins H, Conner D, Thierfelder L, Jarcho JA, MacRae C, McKenna WJ, Maron BJ, Seidman JG, and Seidman CE.** Mutations in the cardiac myosin binding protein-C gene on chromosome 11 cause familial hypertrophic cardiomyopathy. *Nat Genet*, 11: 434-437, 1995.
100. **Watkins H, McKenna WJ, Thierfelder L, Suk HJ, Anan R, O'Donoghue A, Spirito P, Matsumori A, Moravec CS, and Seidman JG.** Mutations in the genes for cardiac troponin T and alpha-tropomyosin in hypertrophic cardiomyopathy. *N Engl J Med*, 332: 1058-1064, 1995.
101. **White HD and Taylor EW.** Energetics and mechanism of actomyosin adenosine triphosphatase. *Biochemistry*, 15: 5818-5826, 1976.
102. **Yang Z, Stull JT, Levine RJ, and Sweeney HL.** Changes in interfilament spacing mimic the effects of myosin regulatory light chain phosphorylation in rabbit psoas fibers. *J Struc Biol*, 122: 139-148, 1998.











